Chapter 7
Intermolecular Interactions and Self-Assembly of Peptide-Based Nanomaterials Against Human Pathogenic Bacteria

Wenbo Zhang, Lanlan Yu, and Chenxuan Wang

Abstract Nanomaterial systems composed of polypeptides are inherently hierarchical in their organization: non-covalent interactions displayed by peptide building blocks engender well-ordered structures with broad applications. This chapter is intended to reflect on the recent progress made in the development of functionalized peptide self-assembling nanomaterials and their therapeutic applications against pathogenic bacteria. We review recent efforts directed to the creation of structurally defined supramolecular assemblies derived from either peptides or synthetic oligomers mimicking the folding and organization of polypeptides. We elucidate the roles of non-covalent interactions, which are encoded by peptide primary amino acid sequence, on the folding and self-assembly of peptides, which in turn gives rise to biological function (e.g., antibacterial activity). Overall, the capability to build peptide-based nanomaterials and tune their functional properties presents exciting opportunities for future research and applications.

Keywords Protein folding · Self-assembled nanostructures · Antimicrobial · Intermolecular interaction · β-peptide

7.1 Introduction

A delicate balance between the host innate immune system and microbes is required to maintain human health. Perturbation of this balance can cause various microbial infectious diseases. Multicellular organisms have evolved immune response mechanisms to defend against the invasion of microorganisms. Host defense peptides are a diverse group of peptides with broad-spectrum activity against gram-positive

W. Zhang · L. Yu · C. Wang (✉)
State Key Laboratory of Medical Molecular Biology, Institute of Basic Medical Sciences, Department of Biophysics and Structural Biology, Chinese Academy of Medical Sciences and Peking Union Medical College, Beijing, China
e-mail: wangcx@ibms.pumc.edu.cn

H. Xu, N. Gu (eds.), *Nanotechnology in Regenerative Medicine and Drug Delivery Therapy*, https://doi.org/10.1007/978-981-15-5386-8_7

bacteria, gram-negative bacteria, and fungi, serving as an evolutionarily conserved mechanism against the infection of microbes [1].

Most host defense peptides adopt one of the following conformations: α-helix (magainin, LL-37, melittin, cecropin), β-sheet (arenicin, PMAP-23, lacidophilin, human β-defensin-2), extended (indolicidin, Bac-5, PR-39, omiganan) [2]. Upon contact with cell membranes, host defense peptides fold and spatially segregate cationic and hydrophobic amino acid residues on opposite faces of the molecule, resulting in amphiphilicity [1, 2]. The amphiphilic nature of host defense peptides thereby allows them to partition into bacterial cell membranes and disintegrate the lipid bilayer structure [3]. Several distinguishable hypotheses have been proposed to interpret the action mechanisms of membrane permeabilization by host defense peptides: barrel-stave, toroidal pore, and carpet [1, 4–6]. In the barrel-stave model, peptides reach the membrane as monomers or oligomers and assemble on the surface of the membrane. In the next step, they insert perpendicularly into the plane of the membrane bilayer and then recruit more peptide monomers to form a transmembrane pore of bundled peptides [1, 5, 6]. In the toroidal pore model, host defense peptides are oriented parallel to the bilayer plane at low peptide concentration. When peptides reach a critical concentration, they co-assemble with lipid molecules and translocate into the membrane. This action disintegrates the membrane and releases micelles composed of a peptide-lipid supramolecular dynamic complex [1, 4]. In the carpet mode, amphiphilic peptides cover the surface of lipid membrane at a high density. When the concentration of host defense peptide is high enough, the membrane curvature of bacterial cell is changed. It leads to the collapse of the structure of the plasma membrane and the formation of peptide-lipid micelles [1, 6].

In view of the prevalence of microbial resistance to commonly used antibiotics, there is a growing interest to develop peptide antibiotics as potential therapeutic applications. Due to their membrane-lytic activity against bacteria, host defense peptides have a low propensity to induce microbial resistance [1, 2, 4]. However, several factors prevent the clinical application of host defense peptides. One of the major limitations of peptides is their high susceptibility to proteolytic degradation and elimination by the reticuloendothelial system and renal filtration [7, 8]. The rapid metabolism and elimination of host defense peptides results in an insufficient lifetime in vivo to reach their therapeutic targets. Another limitation is that high concentrations of defense peptides produce cytotoxicity to host cells. Some host defense peptides are capable of disrupting mammalian membranes and causing mammalian cell lysis. To overcome problems associated with the failure of host defense peptide in application, substantial efforts have been made to improve the bioavailability of peptide drugs by creating nanostructured materials derived from peptides or peptide synthetic analogs [9, 10]. The strategies that develop nanostructured peptide materials, which include building self-assembled peptide-based nanostructures, encapsulating peptides in a delivery system, and chemical modification, have been shown to improve the peptide stability and delivery to the target [9, 10]. This chapter reviews the recent approaches on the development of new self-assembled peptide-based materials that may challenge the medical fight against pathogenic bacteria.

7.2 Development of Peptide-Based Materials with Antibacterial Activity

Peptide-based building blocks serve as applicable platforms to construct supramolecular nanostructures with high order and complexity. Peptide nanostructures exhibit promising features for broad therapeutic applications, such as nanofiber scaffolds, regenerative medicine and tissue engineering, scaffolds for three-dimensional (3D) cell cultures and 3D cell migration, and to stabilize diverse membrane proteins [11–14]. Herein, we focus on the discussion of peptide-based supramolecular assemblies from the perspective of their designs, characterizations, and potential medical applications against pathogenic bacteria.

7.2.1 Peptide Structures

Prior to the introduction of polypeptide self-assembly-based nanomaterials, it is necessary to give a brief introduction to the basic components of polypeptide structures. Polypeptide chains are formed by linearly linked amino acids in a definite sequence. The amino acid sequence determines protein secondary structure, which reflects the 3D arrangement of protein local segments. The two most common polypeptide secondary structures are α-helices and β structures, though coils and tight turns occur as well. Physicochemical properties of residues determine the characteristics of a protein, including, but not limited to, its 3D structure and its biological function. For example, proline has only one rather than two variable backbone angles and lacks the normal backbone NH. It has stronger stereo chemical constraints to disrupt the regular secondary structures that cause a turn along a protein chain relative to other types of amino acids. Thus, proline is usually located at the edges of a protein although it has hydrophobic properties to some extent. As for glycine, which has the smallest side group that puts little stereochemical constraints on the flexibility of backbone conformation, it is frequently found in a region where main chains are packed close to each other and have a potential to switch backbone conformation. As for other residues, the hydrophobic residues provide relatively strong driving forces for protein folding and are usually buried in the protein interiors, whereas residues with charged side chains (e.g., arginine, lysine, aspartic acid, and glutamic acid) are relatively hydrophilic and are often exposed on the surface of a protein.

7.2.1.1 Helices

α-Helix is a classic element of protein structure. It was first described by Pauling in 1951 as 3.6_{13}-helix in which every backbone NH group donates a hydrogen bond to the backbone CO group of an amino acid located four residues earlier along the

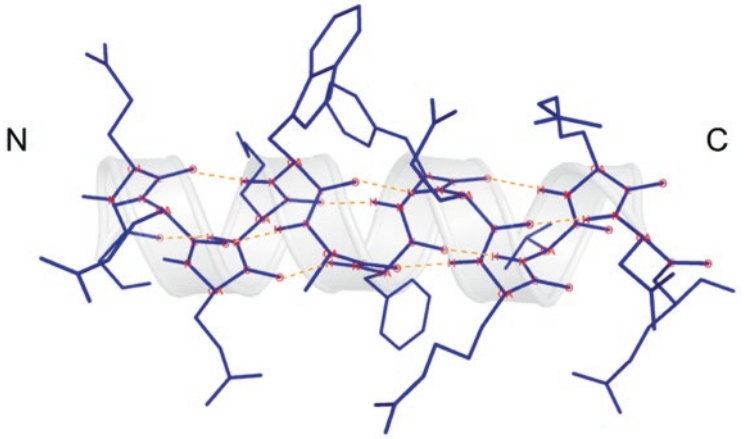

Fig. 7.1 A typical α-helix, residues 114–126 of the arsenate reductase from *Bacillus subtilis* (*B. subtilis*) [16]. The hydrogen bonds between the NH group of residue *n* and the CO group of residue *n-4* are shown as dotted lines in orange. The N- and C-termini of the peptide segment are labeled in the diagram. The direction of view is from the solvent. The front face of the helix contains hydrophilic residues whereas the back side is predominant by hydrophobic residues

protein sequence [15]. Including the hydrogen, the average atomic number per turn is 13 atoms, constructing a closed loop formed by the hydrogen bond. With 3.6 residues per turn, the side chains protrude from the α-helix at about every 100° in azimuth, and the rise per residue along the helix axis is 1.5 Å (Fig. 7.1) [15].

Based on the statistical results from a protein structural databank, α-helices are the most abundant form of secondary structure in globular proteins and are widely distributed on the surface of a protein [15]. Figure 7.2 shows the structure of an arsenate reductase which contains several α-helices [16]. Seven helices and four-stranded β-sheet (see below) are packed into an α/β-domain containing a central twisted β-sheet flanked by four α-helices. It is noteworthy that the axis of a helix may be slightly bent. The most common cause of such a bend is the presence of proline. 3_{10}-Helices are also found at either N- or C-terminal motifs of arsenate reductase. 3_{10}-Helix is a right-handed helical structure with a three-residue repeated segment and a hydrogen bond between the NH group of residue *n* and the CO group of residue *n-3*, instead of *n-4*. The average atomic number per turn is 10 atoms, which are involved in the closed loop formed by the hydrogen bond. With only 3 residues per turn, the side chains protrude from the α-helix at about every 120° in azimuth and a translation of 2 Å along the axis (Fig. 7.2). Long 3_{10}-helices are rare, but short segments of 3_{10}-helices are frequently found in globular proteins and polypeptides. However, the 3_{10}-helix is considerably less favorable than the 3.6_{13}-helix for a long periodic structure, in connection with the hydrogen bond configuration energy and local conformational energy.

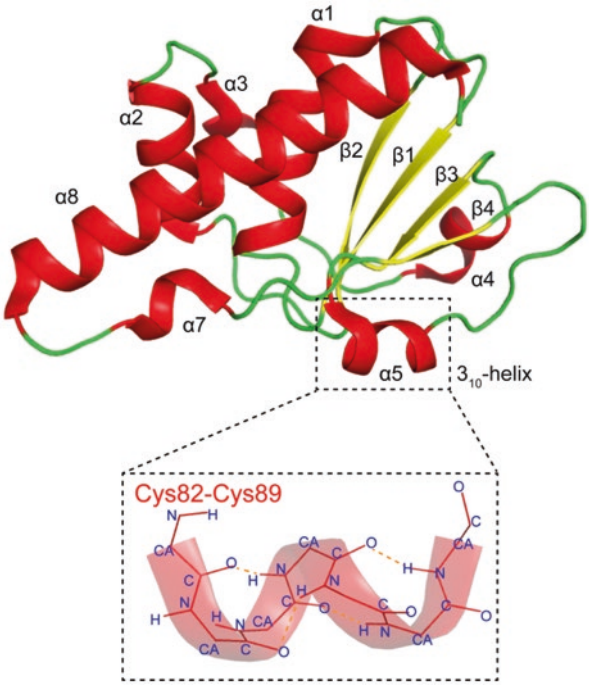

Fig. 7.2 Schematic illustration of the reduced state of arsenate reductase from *B. subtilis*. The seven α-helices and four-stranded β-sheet are colored red and green, respectively. The 3_{10}-helix formed by Cys82-Cys89 are emphasized. Hydrogen bonds between the NH group of residue *n* and the CO group of residue *n-3* are shown as dotted lines in orange

7.2.1.2 β Structure

β-Sheet is another representative structural element that is commonly found in globular proteins. In 1933, β structures were first described by William Astbury as straight, extended chains with alternating side chain directions and hydrogen bonds between the adjacent antiparallel chains. However, Astbury did not have enough data to build a correct model, since whether the peptide bond was planar or not is unclear. In 1951, Linus Pauling and Robert Corey proposed a revised model which described the distinctive patterns of the hydrogen bonding for both antiparallel and parallel β-sheet. This model described the planarity of the peptide bond and revealed that the β-sheets are pleated. β-Sheets consist of several β-strands connected by two or three backbone hydrogen bonds, forming a generally pleated sheet. In the antiparallel β-sheet arrangement, hydrogen bonds are perpendicular to the strands. Successive β-strands alternate directions, and thus the inter-strand hydrogen bonds between the CO groups and NH groups are in a plane, which is their preferred orientation and contributes to the strongest inter-strand stability. This model suggests that the narrowly spaced bond pairs alternate with widely spaced pairs. In the parallel β-sheet

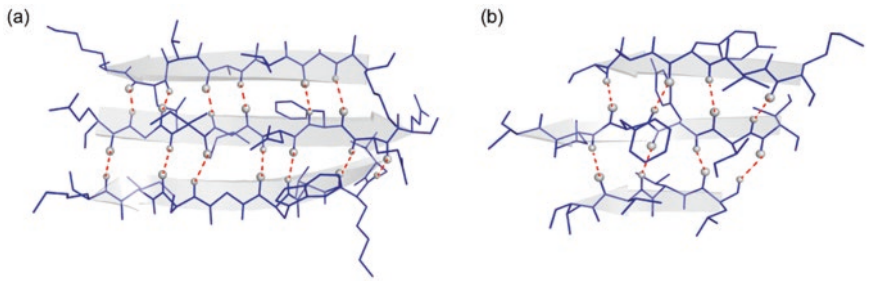

Fig. 7.3 Representative antiparallel and parallel β-sheets. (**a**) An example of antiparallel β-sheet from arsenate reductase (PDB code: 1Z2D) (residues 5–10, 33–37, and 77–80). (**b**) An example of parallel β-sheet from Cu/Zn superoxide dismutase (PDB code: 1DSW) (residues 3–9, 15–22, and 29–36). The directions of each strand are shown by arrows. The hydrogen bonds are shown by dotted lines and the atoms involved are shown as spheres

arrangement, successive β-strands are oriented in the same direction and generate nonplanarity in the inter-strand hydrogen-bonding networks. Figure 7.3 is a schematic illustration of the antiparallel and parallel β-sheets from real proteins.

β-Strands can form a pure antiparallel sheet, a pure parallel sheet, or a mixed sheet composed of both antiparallel and parallel strand pairs. Mixed sheets are relatively instable because the formation of two types of hydrogen bonds requires different backbone orientations, and the standard free energy of formation is relatively unfavorable. In general, a parallel β-sheet is more regular than an antiparallel sheet. It is difficult to find a β-sheet consisting of less than five strands, suggesting that a planar sheet composed of smaller number of strands is unfavorable in energy. However, there are some exceptions. For example, in the structure of arsenate reductase in Fig. 7.2, four β-strands form a parallel sheet exhibiting a twist conformation. Parallel β-sheets and the parallel portions of mixed sheets are always completely buried, with two surfaces of a sheet protected by other main chains (often α-helices). In contrast, an antiparallel β-sheet usually possesses an alternative pattern of hydrophobic/hydrophilic residues in sequence, and thus it exposes one surface to the solvent and keeps one surface in contact with another protein motif. It is notable that large antiparallel sheets can roll up partially or even form a cylinder or a barrel. For example, 5 to 13 β-strands can make up a β barrel, which consists of tandem β-strands twists and coils composed of hydrogen bonds between the first strand and the last strand. Within a β barrel, hydrophobic side chains are pointed toward the interior of barrel, and the barrel can be stabilized by hydrophobic forces. The side chains of hydrophilic residues are always oriented toward the outside of barrel and interact with solvent.

7.2.1.3 Other Nonrepetitive Structures

Helix, β structure, and coil are regular classifications used to describe protein structures. The main feature of coil structure is its nonrepetition in backbone conformation. Coil, commonly referred to as random coil, is a class of conformations without

regular secondary structure. We comment that peptide segments folded to ordered but irregular structures should be distinguished from random coil. For example, β turn, β bend, reverse turn, hairpin bend, kink, and widget are prevalent in protein's non-regular secondary structures. A β turn usually consists of 4 residues (*n*, *n + 1*, *n + 2*, and *n + 3*) and possesses an intra-backbone hydrogen bond between the CO of residue *n* and the NH of residue *n + 3*. The role of β turn is to connect successive β-strands, but sometimes it also appears at the ends of α-helices [15]. Relative to β turn, random coil is a kind of simple unfolded polypeptide chain conformation without any 3D structure.

7.2.2 Self-Assembly of Peptides to Nanostructures

This section focuses on introducing the formation of different self-assembled nanostructures, including their 3D structures, the driving force of the self-assembly, and some manually designed assembly materials. Self-assembly is a process in which the disordered pre-existing components form highly ordered structures controlled by the local interactions among the components' molecules. In aqueous environments, the self-assembly process is mediated through non-covalent forces, including van der Waals interactions, hydrophobic interactions, electrostatic interactions, and hydrogen bonds. Temperature, pH, and solute concentration also influence the self-assembly processes [17].

Many self-assembled molecules possess both hydrophobic and hydrophilic moieties and display amphiphilicity. In a biological system, the most well-known self-assembly structure is the lipid bilayer structure composed of amphiphilic phospholipids which have a hydrophilic phosphate head and a hydrophobic fatty acid tail. In aqueous solution, the nonpolar domains presented by the fatty acid chains engage in hydrophobic interactions to drive self-assembly. The phosphate head groups are largely deprotonated under physiological conditions and thus provide charge-related repulsions. As a result, phospholipids assemble into a two-layered sheet in which the hydrophobic tails point toward the center of the sheet and phosphate head exposed to water. The self-assembly of polypeptides or proteins is more complicated due to their complex amphiphilicity. For example, the side chains exposed on two faces of a β-pleated sheets can be either hydrophilic or hydrophobic. The folding and assembly of polypeptides is governed by the non-covalent networks that arise from side chain properties, such as charge, hydrophobicity, size, and polarity. Therefore, the chemical and structural principles encoded by amino acid identity provide an invaluable handle for manipulating and designing self-assembled polypeptide structures and peptide-peptide interactions. Here, we discuss a few representative supramolecular arrays by using peptides or proteins and unveil the principles of designing polypeptide building blocks (Fig. 7.4).

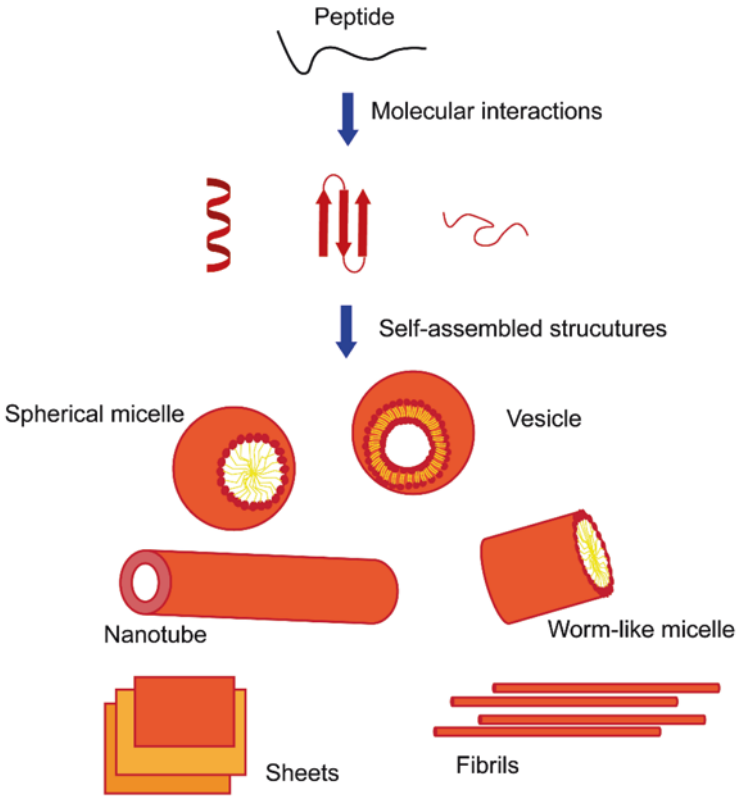

Fig. 7.4 Representative self-assembled structures, including spherical micelle, vesicle, worm-like micelle, nanotube, sheet, and fibril. The hydrophilic head and hydrophobic tail are represented as red spheres and yellow sticks, respectively

7.2.2.1 Tubular Nanostructures

Nanotubes are elongated tube-like structures and have a defined inner hole. The driving forces of nanotube growth originate from hydrogen bonds and π–π stacking of aromatic residues (cyclic peptides), as well as hydrophobic interactions (peptide amphiphiles).

Ghadiri and coworkers demonstrated a strategy to rationally design hollow nanotubes by using heterochiral cyclic peptides [18]. They used D- and L-amino acids to synthesize a cyclic heterochiral octapeptide cyclo[-(D-Ala-Glu-D-Ala-Gln)$_2$-] that self-assembled through hydrogen bonds. When the side chain of E is protonated, cyclic peptides are stacked into an antiparallel β-sheet like conformation, via hydrogen bonds between peptide backbones, and crystallize into tubular structures about hundreds of nanometers long with a 0.7–0.8 nm pore size. The hollow nanotubes made up of cyclic peptides adopt a specific orientation where

side chains are pointed outward from the nanotube surface, and intermolecular hydrogen bonds are parallel to the long-axis of the tube (Fig. 7.5) [18]. The biological functions of cyclic peptide hollow nanotubes were exploited by Fernandez-Lopez and coworkers [19]. The cyclic peptide family was found to potentially self-assemble in bacterial membranes and increase the membrane permeability. As a result, this kind of β-sheet-like tubular architecture exhibits promising antibacterial activity against gram-positive bacteria (*Bacillus subtilis*, *Bacillus cereus*, *Staphylococcus aureus*, *Listeria monocytogenes*) and gram-negative bacteria (*Enterococcus faecalis*, *Streptococcus pneumoniae*) [19].

Nanotubular structures can also be achieved by using peptide amphiphiles which have a hydrophobic tail and a hydrophilic head. Usually a bioactive peptide amphiphile also has a section of charged amino acids to promote solubility and bioactive functional peptide epitope (Fig. 7.6) [20]. The hydrophobic tails can be oligomers

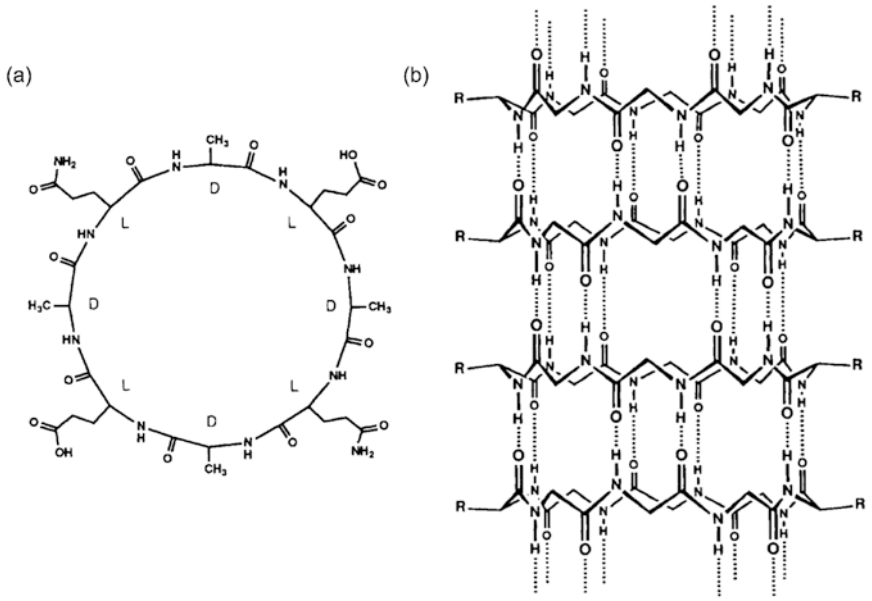

Fig. 7.5 (**a**) The chemical structure of cyclo[-(D-Ala-Glu-D-Ala-Gln)$_2$-]. The "D" or "L" represents the amino acid chirality. (**b**) Peptide subunits are shown as self-assembled tubular structures. The antiparallel stacking and the hydrogen-bonding interactions network are emphasized [18]

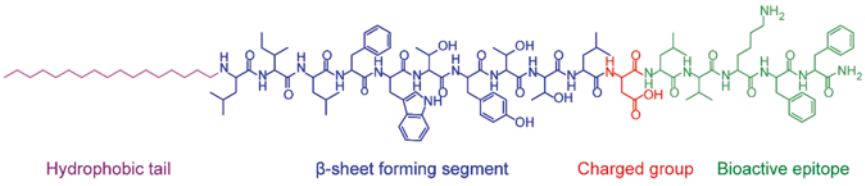

Fig. 7.6 A typical structure of peptide amphiphile. The four domains incorporate into the bioactive β-sheet peptide amphiphile [20]

of nonpolar amino acids (G, A, V, I, L, P, and F), while the heads are normally composed of positively charged amino acids (H, K and R) or negatively charged amino acids (D and E). Both the hydrophobic interactions generated by nonpolar tails as well as the hydrogen bonds between peptides provide attractive interactions for the assembly of peptide amphiphiles. For example, A_mK (where m = 3, 6, and 9) is a typical kind of peptide amphiphile. A_3K forms β-pleated sheet structure via hydrogen bonds, whereas A_6K forms long nanotubes and A_9K forms short nanorods which are driven by hydrophobic interactions [21, 22].

7.2.2.2 Nanofibers

Fibers with a diameter size of less than 100 nm are called nanofibers. The main difference between the nanofibers and nanotubes is that nanotubes include hollow structures while nanofibers do not. Under some specific solution conditions (temperature, pH, and ionic strength), peptides assemble into nanofibers via interpeptide hydrogen bonds and hydrophobic interactions. Stupp and coworkers created a broad class of 3D networks composed of nanofibers by using amphiphilic peptides, such as IKVAV [23]. Hamley and coworkers found that an alanine-rich peptide $A_{12}R_2$ can form twisted nanofibrils by stacking polyalanine domains [24]. Peptides in β-sheet conformation with alternating hydrophobic and hydrophilic residues can also form nanofibers. For example, alkylated peptide amphiphiles $C_{16}H_{31}$OVEVE, consisting of hydrophobic and negatively charged residues and an alkyl chain, can self-assemble into flat nanobelt structures (Fig. 7.7) [20].

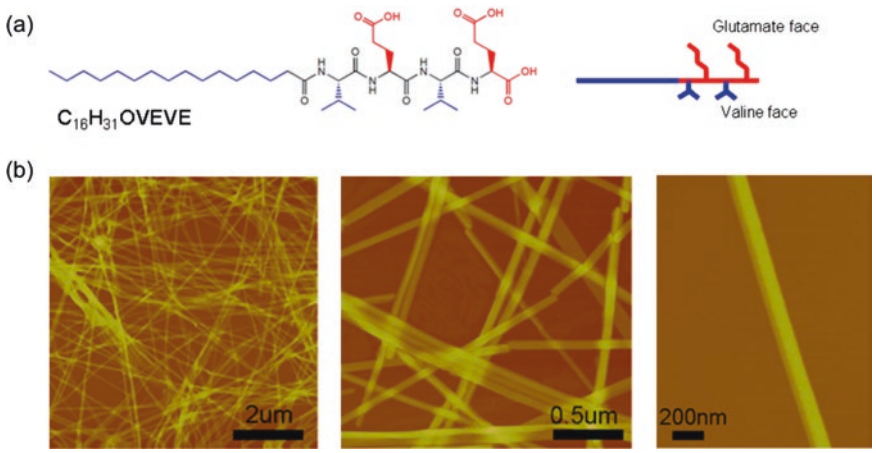

Fig. 7.7 Nanobelts assembled from a peptide amphiphile $C_{16}H_{31}$OVEVE. (**a**) Chemical structure of the peptide amphiphile. (**b**) AFM images of peptide nanobelts. Reprinted with permission from [20]. Copyright 2009 American Chemical Society

7.2.2.3 Spherical/Vesicle Structures

In aqueous solution at neutral pH, amphiphilic oligopeptides consisting of different proportions of hydrophilic to hydrophobic block length can self-assemble into spherical or vesicular structures. The peptides that self-assembled into vesicles were proline-rich peptides, copolypeptides, and cyclic peptides. Deming and coworkers showed that the poly(L-lysine)-b-poly(L-leucine), poly(L-glutamic acid)-b-poly(L-leucine), and poly(L-arginine)-b-poly(L-leucine) diblock polypeptides (where "b" refers to block) exhibit self-assembly behaviors, and stable vesicles and micelles are formed by the charged amphiphilic block copolypeptides [25]. The α-helical hydrophobic rod formation of the poly(L-leucine) block contributes to the formation of diblock polypeptides. Dreher and coworkers reported that self-assembly of elastin-like polypeptides, which were temperature triggered, can form spherical micelle architecture. Elastin-like polypeptides (ELPs) in a linear AB diblock architecture exhibit temperature-triggered self-assembly through a small increase in temperature between 37 and 42 °C [26]. While 37–42 °C is commonly used for clinical application of hyperthermia, spherical micelles formed by ELPs are used in drug therapy. Besides, both the length of the copolymer and the hydrophilic/hydrophobic block ratio control the size of the micelle. Lee and coworkers designed a block polypeptide of polyproline and an arginine oligomer, $P_{10}R_3$, which can form vesicles rather than micelles [26].

7.2.3 Structural Characterization of Self-Assembled Peptides

A series of experimental approaches, such as X-ray diffraction, nuclear magnetic resonance (NMR) spectroscopy, and cryo-electron microscopy (Cryo-EM), have been used to characterize polypeptide self-assembly structures under various conditions and study the interactions among peptides and proteins.

7.2.3.1 X-Ray Diffraction

Single crystal X-ray diffraction is the most unambiguous method for determining the arrays of atoms and molecules within a protein, which is based on the scattering of X-ray waves by electrons in the crystal. X-rays are electromagnetic waves with a wavelength of only around 1 Å. In 1895, Wilhelm Conrad Röntgen developed the method of protein crystallography inspired by the discovery of X-ray. In 1912, Max von Laue observed the diffraction of X-rays by a crystal and demonstrated that the scattering pattern would mark out the symmetrical arrangements of atoms in the crystal. These discoveries were followed by William and Lawrence Bragg, father and son, who invented the X-ray spectrometer and founded X-ray crystallography for the analysis of crystal structure. After 45 years of hard work, John Cowdery

Kendrew and Max Perutz solved the first crystal structure of a protein (the sperm whale myoglobin). They shared the Nobel Prize in Chemistry in 1962. So far, over 150,000 protein crystal structures have been deposited in the PDB databank, as well as the nucleic acids and other biological molecules. Several protein crystallographic structure studies have been awarded the Nobel Prize, illustrating the high level of recognition these outstanding works hold in the academic world. Some examples include the prize awarded to Dorothy Hodgkin (Chemistry Prize of 1964) for the determination of the structures of vitamin B_{12} and insulin; Johann Deisenhofer, Robert Huber, and Hartmut Michel (Chemistry Prize of 1988) for their efforts in solving the structure of the photosynthetic reaction center (first membrane protein); John E Walker (Chemistry Prize of 1997) for the structure of ATP synthase; Peter Agre and Roderick MacKinnon (Chemistry Prize of 2003) for their research on ion channels in cell membranes; Roger Kornberg (Chemistry Prize of 2006) for his protein crystallography-related study of molecular basis or RNA transcription machinery; Venki Ramakrishnan, Thomas A. Steitz, and Ada Yonath (Chemistry Prize of 2009) for the determination of the structure of the ribosome; and Brian Kobilka and Robert Lefkowitz (Chemistry Prize, 2012) for revealing the function and structures of GPCR proteins.

Figure 7.8 illustrates the workflow of protein crystallography. When using X-rays to detect the structures of proteins, the protein or polypeptides need to be first purified and crystallized. The preparation of well-diffracting single crystals is a time-limiting step. Hundreds to thousands of conditions need to be screened to optimize the expression, purification, and crystallization conditions of a specific polypeptide. Once appropriate protein crystals are obtained, it is necessary to submit them to the diffraction data collection process. The crystal is repeatedly exposed to X-ray beams in different orientations. Depending on the type of protein or polypeptide crystal (the cell size and symmetry), different strategies are employed for data collection, and different amounts of scattered X-rays are collected. When an X-ray beam hit a crystal, the X-ray diffraction occurs. All of the electrons in a crystal are hit with an X-ray and all of these electrons then diffract X-ray waves in all directions. Each electron in the sample can also become a small X-ray source. When the scattered waves from all electrons of each atom are added, they can either interfere constructively or destructively. The diffracted waves which get stronger are recorded by X-ray detectors. Finally, by measuring the angles and intensities of these diffracted beams, a 3D image of the density of electrons within the crystal is produced by a crystallographer, with each compound having a unique diffraction pattern. Flexible portions of a protein are often invisible in crystallographic electron density maps, because their electron density is smeared out over a large volume, which is known as a truncated error. The diffraction data is processed by using specialized computer programs, which provide the phase information of the X-ray wave in each spot and the electrons distribution in protein. The processed electron density map is informative, demonstrating positions of atoms, chemical bonds, and other valuable information in a crystal. Finally, one can reconstruct the position of each atom in a crystal by observing the diffraction pattern and build the 3D map of macromolecule. The protein or polypeptide structures are available to all scientists in a public database

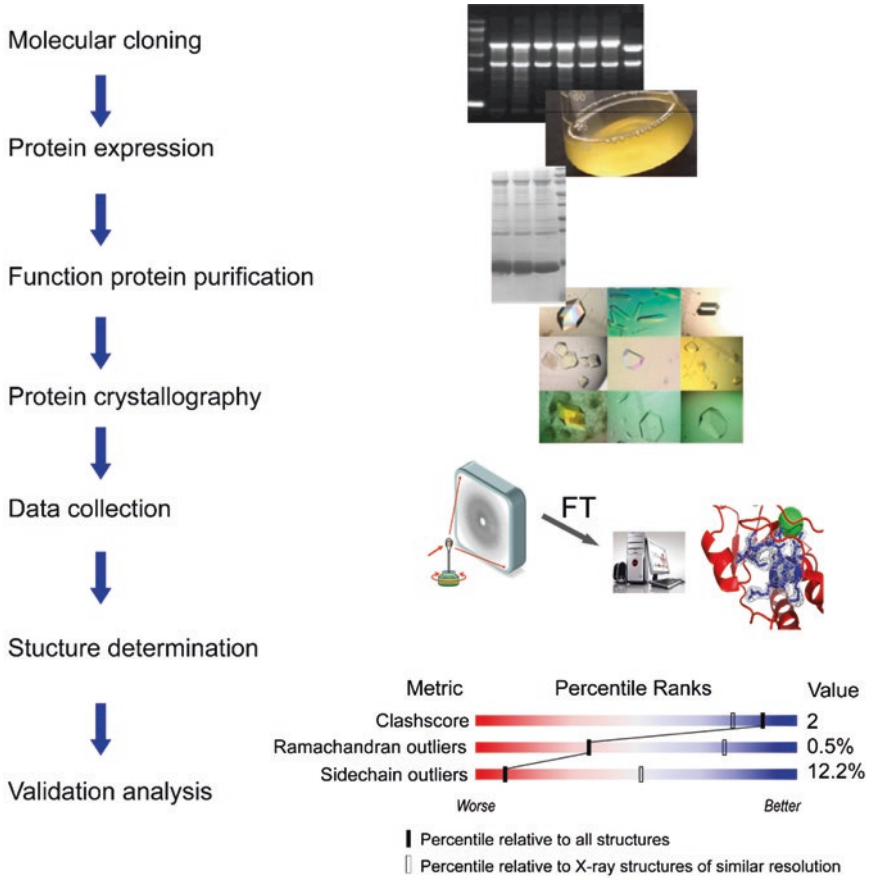

Fig. 7.8 The workflow of protein crystallography

called the "Protein Data Bank" (PDB) with detailed coordinate information and research methods.

Using X-ray crystallography, Eisenberg and coworkers studied the molecular mechanism of insulin amyloid fibrosis. A variety of amyloid fibrils are proteins that are misfolded into β-sheet conformation and form aggregated filaments 6–12 nm in diameter with variable lengths. Researchers obtained the fibril-like microcrystalline aggregates of the segment from insulin B-chain (LVEALYL) and determined the atomic arrays within the LVEALYL microcrystals. X-Ray crystallography yielded a resolution of about 1 Å, which provides information about the peptide structure and the fibrillization process of amyloidal peptide (Fig. 7.9). The peptide adopts a hydrogen-bonded cross-β-conformation, like a continuous stack of β-sheet ladders. Segments LVEALYL with extended strands conformation pack into parallel β-sheets, and each pair shows the dry steric zipper interface typical of amyloid-like fibrils [27].

Fig. 7.9 Atomic structure of the insulin dimer (PDB code: 1GUJ) [27]

By using similar methodology, Eisenberg and coworkers revealed two potential mechanisms for prion strain propagation based on the structure determination of the segments from prion and other amyloid proteins [28]. Prions are a kind of infectious proteins that can cause transmissible neurodegenerative diseases in mammals and produce heritable and sometimes beneficial phenotypes in fungi. In the inheritance and transmission of prions, strains are phenotypic variants encoded by protein conformations. Structural conversion from soluble to amyloid-like structure rich in β-sheets (aggregated) is involved in the process of prion formation. The aggregated prion accelerates the conversion of identical soluble protein molecules to the status of aggregation. However, the mechanism of maintaining protein structure stability in enduring transmission between cells or organisms is still unclear. Conformational differences that give rise to polymorphic amyloid fibrils and prion strains at atomic level are poorly understood. Researchers have determined that the steric zipper structures of fibril-like amyloidal protein segments are polymorphous (Fig. 7.10a). The different phenotypes of prion strains reflect changes in the conformations of steric zippers (Fig. 7.10b). Prion strains can be encoded by alternative packing arrangements of β-sheets, which are formed by the same segment. At the same time, prion strains can also be encoded by distinct β-sheets of different segments. The above two forms of polymorphism produce combinatorial conformations and transfer protein-encoded information into prion strains.

The X-ray crystallography progress to explore polypeptide assembly structures is evident, while challenges still remain relating to the flexible portions of protein. A polypeptide that is highly dynamic in solution with a nearly free rotation and tilt angle is difficult to be studied by X-ray crystallography, since the electron density in highly flexible regions is largely weakened in X-ray diffraction. To gain information with such a system, NMR spectroscopy can be used as a suitable characterization technology.

7.2.3.2 NMR Spectroscopy

NMR spectroscopy is the second method for determining protein structures with atomic resolution and has led to a substantial increase in the number of known protein structures. NMR is a nuclei-specific spectroscopy that measures the energy gap

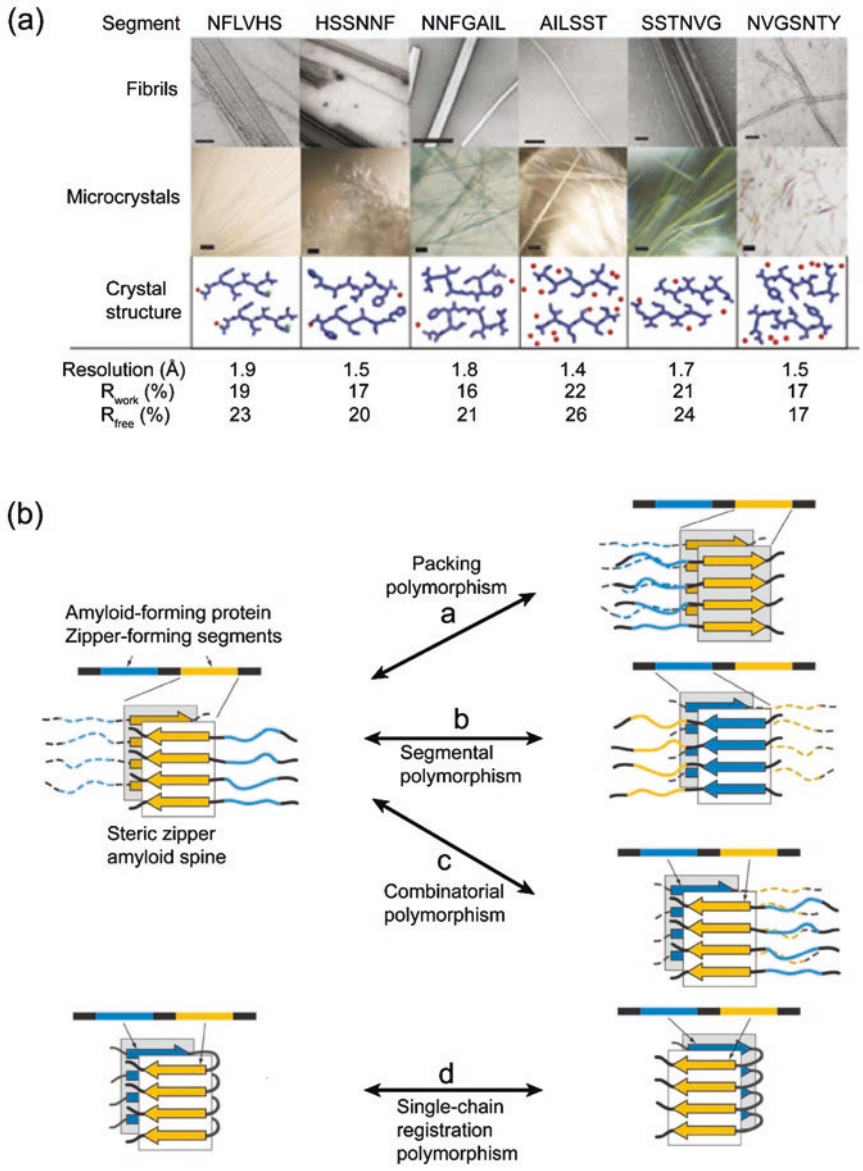

Fig. 7.10 Polymorphism in islet amyloid polypeptide (**a**) and the schematic diagram of steric zipper mechanisms for amyloid and prion polymorphism (**b**). (**a**) Peptide segments were detected to form fibrils, as shown in the electron micrographs above (scale bars are 100 nm). The segments also form microcrystals, as shown in the center (scale bars are 50 μm) of light micrographs. Crystal structures of the segments were also determined, and the resolutions and *R* factors are represented below. (**b**) Two segments in an amyloid-forming protein are respectively depicted in blue and yellow. Reproduced from [28]

between spin-up and spin-down states of nuclei in an external magnetic field. NMR techniques can provide many complementary information to those obtained from X-ray crystallography, including the atomic local structures of highly flexible regions and protein dynamic properties. Thus, NMR techniques broaden our view of molecules and give us a profound insight into the relation between structure, dynamics, and biological function. In the late 1960s and the early 1970s, with the rapid development of modern NMR techniques, including Fourier transform spectroscopy, superconducting magnets, new pulse programs, and computer control of the instrumentation, NMR spectroscopy has emerged as a powerful technique to characterize protein structures in solution. NMR has been used to study protein internal mobility, conformational changes, folding processes, pH titration of individual amino acids in protein-protein or protein-ligand interactions, and the atomic resolution structure of proteins.

Figure 7.11 presents an outline of the NMR method, including protein sample preparation, NMR experiment data collection, atom assignment, and structure calculation. The protein of interest is usually dissolved in aqueous solution (0.4–0.5 mL) under near-physiological conditions. The appropriate protein concentration is higher than 0.3 mM, ideally around 1 mM. For proteins larger than 12 kDa, samples should be ^{15}N and/or ^{13}C labeled. To collect NMR spectra of proteins, two-dimensional (2D), three-dimensional (3D), or even four-dimensional (4D) experiments are used to avoid extremely crowded and overlapped regions within the one-dimensional ^{1}H NMR spectrum generated by the larger number of hydrogen atoms in a protein. As shown in Fig. 7.11, the cross-peaks, which indicate couplings between nuclei pairs, have been further spread out along the third frequency axis, corresponding to the NMR frequencies of labeled spins. Routine experiments include 2D ^{1}H-^{15}N, ^{1}H-^{13}C HSQC, 3D HNCA, HNCO, HN(CA)CO, HN(CO)CA, HNCACB, CBCA(CO)NH, HBHA(CO)NH, (H)CCH-COSY, HCCH-COSY, and ^{15}N-edited TOCSY-HSQC spectra. Using these spectra, one can assign the frequencies at which energy absorption occurs for each of the specific NMR active nuclei in the sample. For a de novo structure determination, NMR distance constraints are obtained from nuclear Overhauser enhancement (NOE) spectroscopy, called NOESY. In the NOESY experiment, a cross-peak between two hydrogen atoms is observed only if the distance between the two protons is shorter than 6 Å. As the NOE depends on distance, one can use these distance constraints to build protein structure. Other NMR experiments can also provide distance or angle constraints, such as residual dipolar couplings (RDCs) and paramagnetic resonance enhancement (PRE) experiments. A RDCs experiment measures weakly aligned macromolecules dissolved in dilute liquid crystalline media and provides long-range orientational information that leads to significant increases in coordinate accuracy [29, 30]. The PRE effect, arising from unpaired electrons with an isotropic *g*-tenser (such as EDTA-Mn^{2+}/EDTA-Cu^{2+} or a nitroxide spin label), provides long distance (10–35 Å) restraints according to the PRE between the paramagnetic center and the nucleus [31]. PRE structures are calculated using specific computational programs. Dihedral angles (φ and ψ) can be predicted from chemical shifts using the program TALOS. The CANDID module of CYANA was used to generate the initial structure. About 20 structures with the lowest target functions are selected as models for

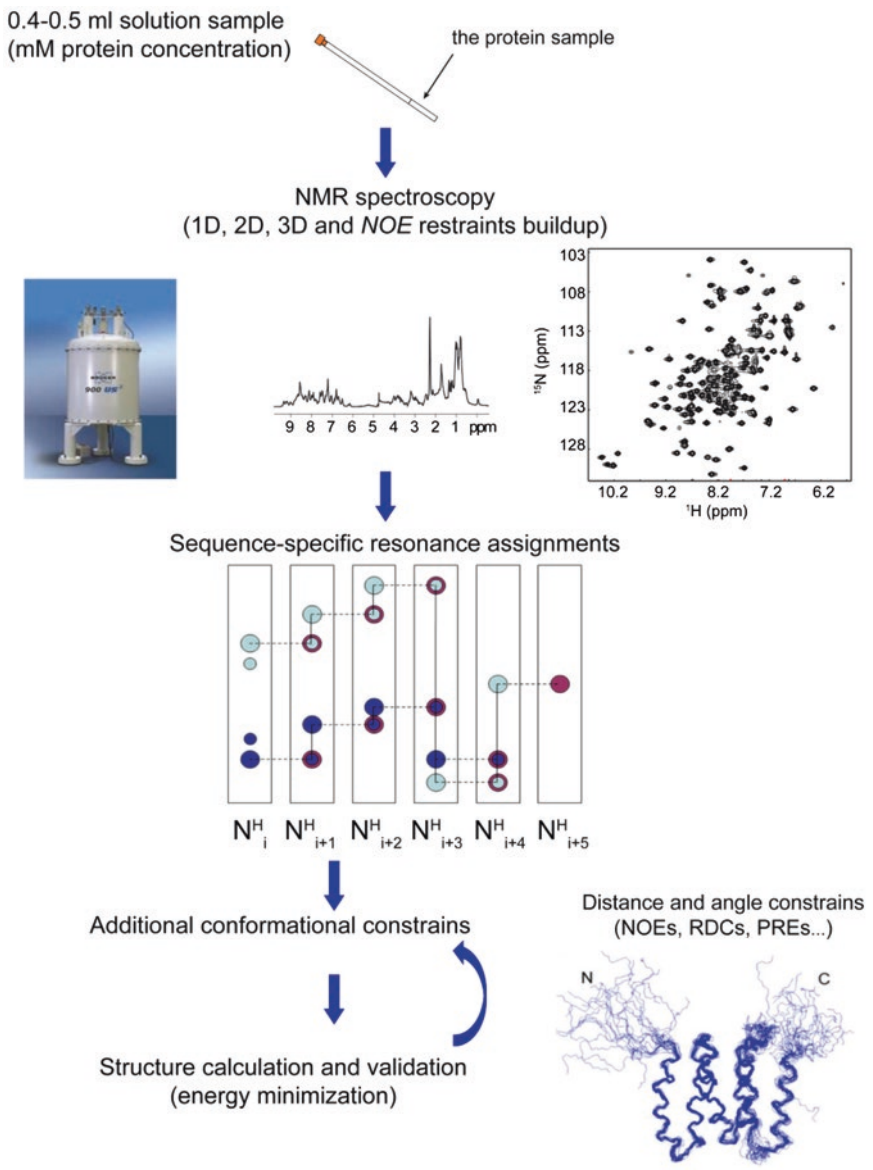

Fig. 7.11 The workflow of using the solution NMR to detect proteins structures

the program SANE to extend the NOE assignments. 200 structures are first calculated by CYANA interactively, and the 100 lowest energy structures then selected for further refinement by AMBER. Finally, 10–20 conformers with the lowest energy are selected to represent the solution structure. The quality of calculated conformers can be checked by analyzing the violations using PROCHECK software programs.

^{1}H, ^{13}C, ^{15}N triple resonance 3D and 4D spectroscopy have extended the size limit of protein NMR to 25 kDa. However, compared with other techniques, the molecular size of proteins that can be studied by NMR is relatively small. The main reasons are as follows: (1) NMR signals rapidly decay during the multitude of transfer steps in an NMR experiment; (2) The spectra become too crowded as protein molecular weight increases; (3) Cross-peaks in NOE-type spectra increase rapidly with size. These problems can be generally eliminated by employing novel techniques, such as the transverse relaxation-optimized spectroscopy (TROSY), PRE, RDCs, and pseudo-contact shifts (PCS). Labeling strategies involving perdeuteration and methyl-specific labeling of ILVs also allow researchers to obtain key structural restraints for larger proteins.

The methods mentioned above are NMR methodologies working in solution. Another type of NMR technique is solid-state NMR (ssNMR). The principle of ssNMR is the same as that of solution NMR. The ssNMR is widely used in analyzing membrane proteins inserted into lipid bilayers, which provides crucial structural and functional information of the membrane proteins. The orientation dependence of NMR interactions under non-spinning condition is exploited. The rigid-body structure of a peptide nanotube adopts a unique orientation when it is supported on glass slides. Thus, it is feasible to probe the orientation of peptides within a nanotube framework. Hamley and coworkers provided structural insights into the conformation of nanotube forming peptide H_2N-AAAAAAK-COOH (A_6K) via ssNMR. By using the unoriented A_6K nanotubes sample labeled with 1-^{13}C Ala at residue 2 and 2-^{13}C Ala at residue 6, they found that A_6K peptides are arranged in an antiparallel β-sheet within the nanotubes. Their results demonstrated that A_6K nanotubes are 20 nm in diameter and consist of β-strands with a 4.7 Å spacing in the hydrogen-bonding direction. By combining the results from ssNMR experiments and simulations, a series of structural models was proposed to be that A_6K β-strands are packed perpendicular to the nanotube axis to form a belt with a twisted angle θ in the range of 65–70° (Fig. 7.12) [32].

7.2.3.3 Cryogenic Electron Microscopy

Cryo-EM provides a feasible method to study the structures of large or heterogeneous proteins and biological macromolecular assemblies, which are difficult to be investigated by using conventional X-ray crystallography or NMR techniques. In a

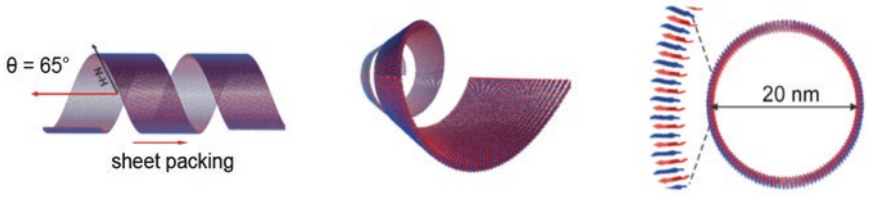

Fig. 7.12 Three perspectives of the nanotubes formed by peptide A_6K. Reprinted with permission from [32]. Copyright 2013 Wiley Publishing Group

cryo-EM experiment, biological specimens are frozen-hydrated at cryogenic temperatures and remain in their native state without the use of dyes, fixatives, or crystallization. It provides high-resolution structures of cells, viruses, and protein complexes. In the 1960s, scientists were faced with the problem that when using electron microscopy to study the structures of biomolecules, the high energy electron beams damaged the specimen. To overcome this problem, cryo-EM was invented, as it was expected to reduce the beam damage due to the low environment temperatures. In 1975, Joachim Frank proposed algorithms that can analyze 2D images and reconstruct them into 3D structures. In the early 1980s, Jacques Dubochet devoted himself to vitrify water by quickly cooling samples. This process allows the biomolecules to retain their shape in a vacuum. In the 1990s, Richard Henderson used electron microscopy to generate the first 3D image of a protein at atomic resolution. The Nobel Prize in Chemistry in 2017 was awarded to these three researchers for their efforts in developing cryo-EM.

Figure 7.13 shows the workflow of cryo-EM to detect protein structures. In the sample preparation step, an aqueous protein solution is dropped onto a carbon film-coated transmission electron microscopy (TEM) grid blotted by using a FEI Vitrobot, and then the grid with the sample is rapidly plunged into the mixture of liquid nitrogen and ethane. Frozen proteins are embedded in a thin layer of amorphous ice with a thickness of around 100 nm, which can preserve proteins in a near-native environment. The samples are quickly transferred to a TEM with cryogenic capability, maintaining low temperatures during experimentation (~90 K cooled by

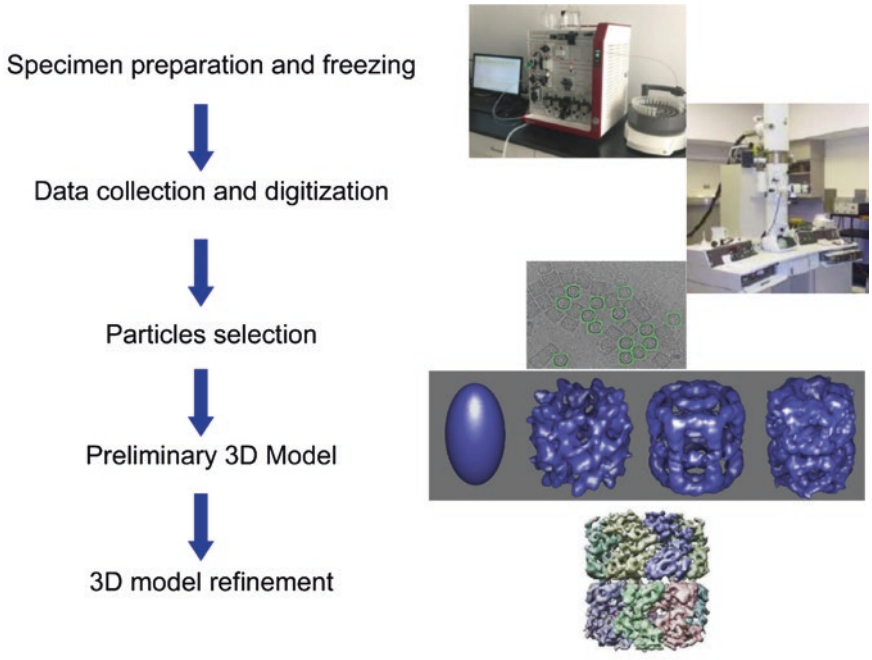

Fig. 7.13 The workflow of using electron cryo-microscopy to detect protein structures

liquid nitrogen, or ~ 4 K cooled by liquid helium). Thus, the protein samples are fixed in a hydrated state in vacuum. Images with high noise level and low contrast are recorded by using electron exposures low enough at low temperature to avoid destroying samples. To get high-resolution structural information, multiple 2D images of the specimen are collected and averaged. To reconstruct the 3D structure of a biomolecule, the single-particle analysis (SPA) procedure was developed by Frank and coworkers [33]. In the SPA procedure, thousands of 2D images of a biomolecule in different orientations are combined to generate a 3D reconstruction. Software packages that are being used in the field of SPA (e.g., EMAN, IMAGIC, Bsoft, Frealign, and RELION) are based on the SPIDER program created by Frank and coworkers in 1981. Any reconstruction process by SPA is built on the assumption that the imaged sample is a homogeneous population of structurally identical and chemically identical objects. However, not all the biological samples are truly homogeneous. Such instances of heterogeneity include the simultaneous presence of multiple biomolecule conformations and the variable nature of a bound ligand. In such cases, one should divide these 2D images into multiple homogeneous sets, and then generate multiple 3D models.

Stupp and coworkers used cryo-EM technique to investigate the structure of cylindrical nanofibers formed by alkylated peptide amphiphiles, $C_{16}H_{31}$OVVEE, which consist of hydrophobic and negatively charged residues (V and E) and a hexadecane tail [20]. Previous works demonstrate that the VEVE segment in a similar peptide $C_{16}H_{31}$OVEVE flips the hydrophilic and hydrophobic side chains to the opposite sides of extended peptide β-strand. The hydrophobic valine residues in the peptide sequence are expected to exhibit a tendency to form a dimer to limit exposure to water. Thus, researchers hypothesized that the alternation of peptide sequence from VEVE to VVEE would lead to a more effective peptide chain packing. Consistent with their prediction, the replacement of the VEVE structural motif by VVEE converts the topology of the peptide self-assembly nanostructure from flat nanobelt to the cylindrical nanofiber (Fig. 7.14).

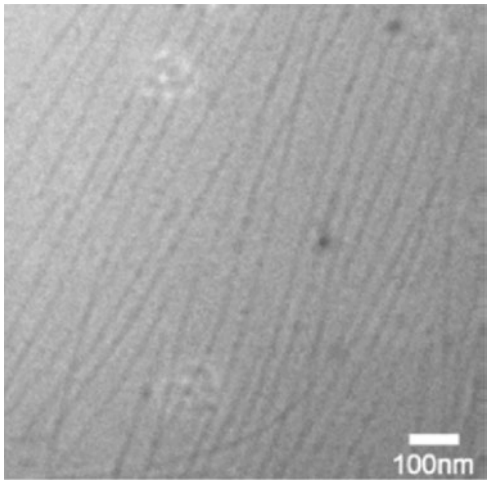

Fig. 7.14 Cylindrical nanofibers in cryo-EM image of 0.1 wt% $C_{16}H_{31}$OVVEE aqueous solution. Reprinted with permission from [20]. Copyright 2009 American Chemical Society

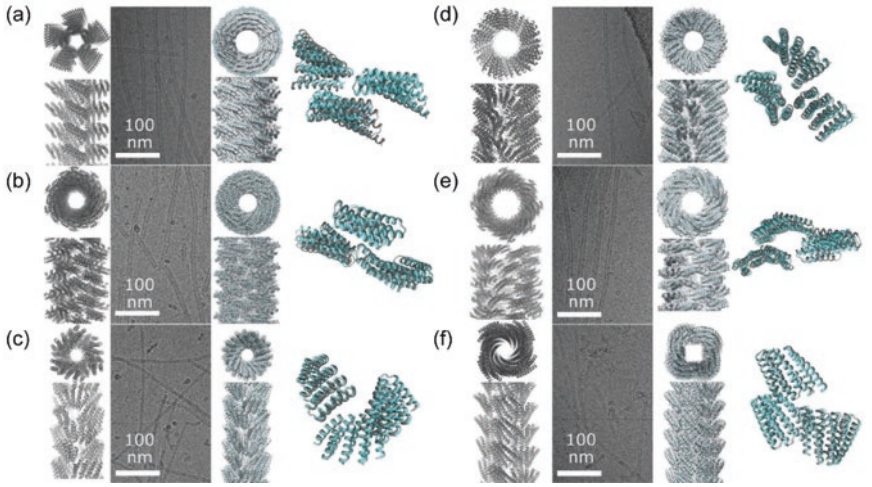

Fig. 7.15 Cryo-EM structures of de novo peptide assembled structures. (**a**–**f**) Computational model, representative filaments in cryo-EM micrographs, cryo-EM structure, and overlay between the model and structure are arranged from left to right. (**a**) DHF58, (**b**) DHF119, (**c**) DHF91, (**d**) DHF46, (**e**) DHF79, and (**f**) DHF38 [34]. Reprinted with permission from [34]. Copyright 2018 The American Association for the Advancement of Science

Cryo-EM techniques are also used to characterize the nanostructures formed by de novo peptides. In 2018, Baker and coworkers described a general computational approach to design self-assembled helical filaments from monomeric proteins [34]. Using this approach, they designed proteins that assemble into micrometer-scale filaments in vivo and in vitro. A set of 15 de novo-designed helical repeat proteins with various geometries was selected as the monomeric building blocks. By using these 15 building blocks, 6 different types of supramolecular architectures with longer persistence lengths were generated (Fig. 7.15). Within these assembly architectures, the overall orientations and packing modes of the monomers in filaments were determined by cryo-EM.

7.2.3.4 Other Methods

A series of other spectroscopic and microscopic technologies also provides us important information about polypeptide assembled structures, including scanning tunneling microscopy (STM), small-angle scattering (SAS), circular dichroism (CD), and multi-angle light scattering (MALS).

The STM works by scanning a surface with a very sharp metal wire tip. When a conducting tip is brought <1 nm to the surface to be examined, a bias applied between the two allows electrons to tunnel through the medium between them. As a result, the surface can be imaged with submolecular resolution by documenting the local density of states. Due to its high structural resolution and adaptability to

various environments, STM has been applied to study the molecular structures of peptides, especially for amyloid peptides that are difficult to be crystallized. In the past decade, STM has provided important details to allow us to gain insights into the assemblies of amyloid-forming peptides, such as human islet amyloid polypeptide, amyloid beta 40 and 42, the key aggregation segment of prion protein, as well as the binding sites of single-drug molecules on peptides [35–38].

SAS, including small-angle X-ray scattering (SAXS) and small-angle neutron scattering (SANS), is used in the structure characterization of biological macromolecules, nanocomposites, synthetic polymers, and alloys. Relative to solution NMR, which is limited by protein size, and X-ray crystallography, which is time-consuming, the SAS measurement is quick and has no significant molecular weight limitation. When combined with other high-resolution analysis methods, SAS provides 3D structures via ab initio reconstructions and hybrid modeling, which can be used in characterizing equilibrium mixtures and flexible systems.

CD is a kind of dichroism that involves circularly polarized light, such as the differential absorption of left- and right-handed light. CD is exhibited by biological molecules due to their dextrorotary and levorotary components. As a consequence, protein secondary structures have distinct CD spectral signatures representative of their structures, making CD a powerful tool in characterizing the structures of polypeptides.

MALS measures the hydrodynamic size of a particle or a protein assembly in Brownian motion from the scattered light intensity collected at multiple scattering angles. This measurement can be used to provide important insights into protein self-assembled structures, protein-protein interactions, and the aggregation status of proteins.

In conclusion, there are many techniques available to study the self-assembly structure of biomolecules. During the research process, scientists sometimes combine various technologies to obtain profound structural insights.

7.2.4 The Application of Self-Assembled Peptide-Based Nanomaterials in the Diagnosis of Bacterial Infection

Speedy diagnosis of a bacterial infection is crucial to the treatment of infectious diseases. Because of the infection complications in the bloodstream, every hour of delay in antibiotic treatment increases mortality rates by nearly 8%. However, the existing physical examination methods, such as microorganism culture and histopathology, and tests for antibodies, antigens, DNA, and RNA, are time-consuming, typically taking up to 2–5 days to obtain accurate and reliable results. Thus, new diagnostic methods are needed to detect the early stage of infection. Self-assembled peptide-based nanomaterials possess distinct biological properties, such as molecular recognition of pathogen attack, biodegradability, and biocompatibility that suggest these materials may be used as sensitive and specific sensors for bacterial detection and infection therapy.

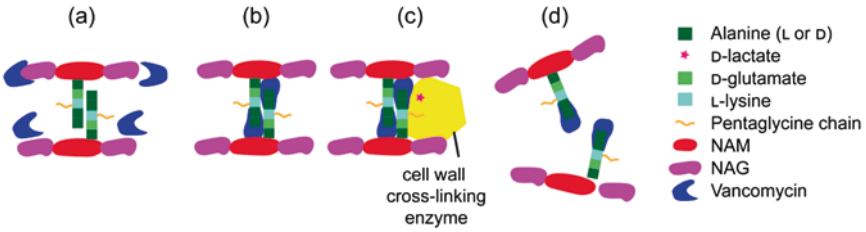

Fig. 7.16 Mechanism of vancomycin action. (**a**) Vancomycin is added to the bacterial environment while bacteria are metabolically active and synthesizing new cell wall. (**b**) Vancomycin recognizes and binds to the D-alanyl-D-alanine moieties on the end of the peptide chains. (**c**) Vancomycin interacts with the peptide chains and prevents them to bind to the cell wall cross-linking enzyme. (**d**) Cross-links cannot be formed and the bacterial cell wall is disrupted

Vancomycin is an antibiotic which is used to treat gram-positive bacterial infections as it can inhibit the proper cell wall synthesis. It is recommended as a first-line treatment for bloodstream infections, endocarditis, skin infections, and meningitis caused by gram-positive bacteria [39, 40]. The gram-positive bacterial cell wall, composed of cross-linked peptidoglycan, is constructed of a repeating disaccharide unit of *N*-acetylglucosamine (NAG) and *N*-acetylmuramic acid (NAM). The NAM bears a peptide moiety L-alanyl-D-isoglutaminyl-L-lysyl-D-alanyl-D-alanine. Vancomycin has been proved to prevent the incorporation of NAM/NAG peptide subunits into the peptidoglycan matrix and thereby inhibits cell wall polymerization by forming hydrogen bonds with the terminal D-alanyl-D-alanine moieties of NAM/NAG peptides (Fig. 7.16).

Inspired by this observation, researchers attempted to develop biotriggered materials with responsive retention and targeting accumulation property. Vancomycin is covalently conjugated with self-assembled peptides or peptide mimetics to design various biosurface-induced supramolecular assemblies for the diagnosis and therapy of bacterial infections.

In 2014, Yang and coworkers reported self-assembled vancomycin derivatives for simultaneous bacterial detection and inhibition [41]. They developed NBD-FFYEGK [Van] and NBD-FFYEEGK [Van] (NBD represents 4-nitro-2,1,3-benzoxadiazole and Van represents vancomycin), which can self-assemble induced by the bacterial surface. While the NBD exhibits the environment-sensitive fluorescence property, the NBD-Van conjugates can be used in bacterial detection and inhibition in vitro. They studied the self-assembly behaviors of these compounds by dynamic light scattering and transmission electron microscopy. The results showed that the critical micelle concentration (CMC) of NBD-FFYEGK [Van] and NBD-FFYEEGK [Van] was 75 and 190 μg/mL, respectively. TEM images of the compound in aqueous solution at pH 7.4 showed that when their concentration was higher than their respective CMC value, both NBD-FFYEGK [Van] and NBD-FFYEEGK [Van] formed nanoparticles. To test their bacterial inhibition capacity, the vancomycin-sensitive strain of *Bacillus subtilis* (ATCC 33677, *B. subtilis*) and vancomycin-resistant enterococci of *Enterococcus faecalis* (VanB genotype, ATCC

51299, *E. faecalis*) were used as model organisms. The antibacterial activity of the two peptide-conjugated compounds was investigated by standard broth microdilution assays. For *B. subtilis*, the minimum inhibitory concentration (MIC) of NBD-FFYEGK [Van] was 4.5 μM, while the MIC of NBD-FFYEEGK [Van] was 22.4 μM. NBD-FFYEGK [Van] (MIC = 90 μM) and NBD-FFYEEGK [Van] (MIC = 213 μM) exhibited more effective antimicrobial activities against *E. faecalis* than the parent vancomycin molecule (MIC = 728 μM). By measuring the local fluorescence intensity of NBD moiety at the bacterial surface, they observed that the formation of NBD peptide self-assembled nanostructures around bacteria increased the fluorescence intensity relative to the environment. It is an interesting observation that bacterial surface functions as an active substrate to recruit free NBD peptides from solution and triggered the onset of assembly of NBD peptides at the bacterial surface.

In 2015, Wang and his group designed a new photoacoustic contrast peptide agent that is capable of self-aggregation triggered by an enzyme in bioenvironments and can be used as a sensitive and specific image sensor for bacterial infection in vivo [42]. The building block is Ppa-PLGVRG-Van 1 (Ppa stands for pyropheophorbide-α, Van stands for vancomycin), where Ppa is a light-sensitive reagent to provide photoacoustic signal and PLGVRG is an enzyme-sensitive peptide linker. Ppa-PLGVRG-Van 1 binds to the gram-positive bacterial cell walls via the hydrogen bonds between vancomycin and D-alanyl-D-alanine moieties. Vancomycin leads Ppa-PLGVRG-Van to accumulate at the site of infection caused by bacteria in vivo. Gelatinase secreted by gelatinase-positive bacteria cuts the PLGVRG peptide linker and releases Ppa to self-aggregate in situ (Fig. 7.17). The aggregates of Ppa are hierarchically twisted fibers with high thermal conversion efficiency for photoacoustic imaging. Hence, the accumulation and aggregation of Ppa-PLGVRG-Van induced by bacterial infection leads to an amplification of the Ppa signal in situ, which can be used as the basis of a highly sensitive and specific system for imaging the bacterial infections. In this research, the self-aggregation and characterization of the supramolecular aggregates were studied by UV-vis absorption spectra, TEM, and CD spectra. To test the function of Ppa-PLGVRG-Van in vivo, a dose of 10^3 to 10^8 bacterial colony-forming units was added to induce muscle inflammation for 24 h. Then Ppa-PLGVRG-Van was intravenously injected (5.0 mg/kg, 200 μL) and the photoacoustic signal was acquired after a further 24 h. The results showed that Ppa-PLGVRG-Van exhibited target accumulation effect in muscles and other organs. Finally, cell viability assays were carried out to examine the toxicity of Ppa-PLGVRG-Van. The experimental data showed that this photoacoustic contrast agent has high biocompatibility as negligible cytotoxicity toward the human embryonic kidney (A293) and human hepatocyte (LO2) cells was observed.

Inspired by the potential of constructing supramolecular self-assemblies in vivo, Liu and coworkers designed a dual fluorescent-radioisotope probe for imaging gram-positive bacterial infection [43]. A vancomycin- and rhodamine-modified peptide derivative (Rho-FF-Van) was synthesized as an imaging reagent and was bound to the D-alanyl-D-alanine motif of the methicillin-resistant *Staphylococcus*

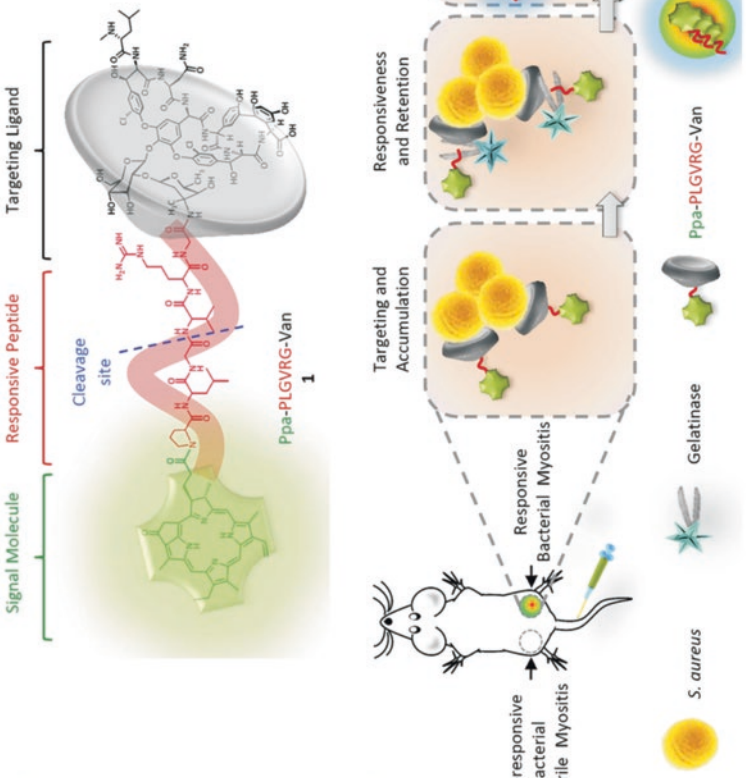

Fig. 7.17 Schematic diagrams of bacterial infection imaging based on an in vivo aggregation strategy. (**a**) The building block Ppa-PLGVRG-Van. (**b**) First, Ppa-PLGVRG-Van accumulates at the site of responsive bacterial myositis with the help of the targeting molecule vancomycin; then, the gelatinase produced by gelatinase-positive bacteria cleaves the peptide linker and triggers self-aggregation in situ; finally, the supramolecular aggregates and makes great contribution to enhance the photoacoustic signal so that the bacterial infection can be detected. Reprinted with permission from [42]. Copyright 2016 Wiley Publishing Group

aureus (MRSA) cell walls. The peptide self-assembled to form nanoaggregates on the surface of MRSA, which resulted in an increased fluorescence intensity at the site of MRSA infection. By measuring the radioactive signal released by the iodine-125 labeled peptide, ^{125}I-Rho-FF-Van, researchers probed bacterial infection in MRSA-infected lung models. Their work provides a novel way to image bacterial infection in vivo. They also synthesized Rho-GG-Van as a control group. To evaluate the self-association potency of Rho-FF-Van versus Rho-GG-Van and determine the appropriate concentration of peptide probes in vitro and in vivo, they compared the CMC values of these peptide probes in PBS buffer. The results revealed that the CMC value of Rho-FF-Van (about 78 μg/mL) is 2.4-fold lower than that of Rho-GG-Van. Similar CMC measurements were conducted with non-rhodamine control groups, Ac-FF-Van and Ac-FF-Van. The presence of rhodamine aromatic ring was observed to facilitate the self-assembly tendency of the peptide. To evaluate the bacterial surface-induced self-assembly of peptide probes, in situ self-assembly of Rho-FF-Van surrounding MRSA surface was visualized by using confocal microscopy and TEM. The results showed that the outer membrane of MRSA treated with Rho-FF-Van exhibited apparent formation of nanoaggregates. In contrast, there was no obvious aggregates formed at the outer membrane of MRSA treated by Rho-GG-Van. These results further confirm that Rho-FF-Van exhibits high sensitivity for the detection of gram-positive bacteria in vitro. Finally, they used myositis-bearing mice that have MRSA on left hind leg and *Escherichia coli* (*E. coli*) on the right hind leg to investigate the ability of Rho-FF-Van for detecting gram-positive bacterial infection in vivo. Rho-FF-Van was administered in the mice intravenously for fluorescence imaging and showed significant fluorescence only on the MRSA-induced infection sites, 2 h post-injection both in vivo and ex vivo.

7.2.5 Application of Self-Assembled Peptide-Based Nanomaterials in the Treatment of Bacterial Infection

The overuse of antibiotics have stimulated the emergence of antibiotic-resistant bacteria; thus, the conventional antibiotics that target individual intracellular processes are facing the barrier of reduced therapeutic potential against pathogens. There are four important pathways leading to bacterial resistance: (1) alteration in the target site of antimicrobial agents to reduce binding affinity, (2) reducing drug accessibility via increasing efflux or decreasing influx, (3) inactivation of a drug by releasing enzymes, and (4) tolerance that results in the survival of bacteria [44, 45]. With traditional search paradigms being exhausted, novel approaches including the creation of antimicrobial peptides and peptide mimetics may offer promising and creative solutions. Naturally occurring antimicrobial peptides are evolutionarily conserved and found in many living organisms. They serve as defense components in the innate immune system against a variety of pathogens. Antimicrobial peptides have some common characteristics as they fold into amphipathic structures in

response to membrane binding. They are cationic and bind to negatively charged bacterial cell membranes by nonspecific physical interactions and cause disrupting pores, channels, or carpets in microbial phospholipid bilayers [1, 4–6]. Although some peptides isolated from natural sources show early success as alternatives to conventional antibiotics, their therapeutic applications are limited by high costs, their low stability to enzymatic degradation in vivo, and off-target cytotoxicity. To overcome these challenges, one possible solution is to use antimicrobial peptides as building blocks and develop three-dimensional hierarchical nanomaterials with wider therapeutic windows.

Webster and coworkers designed a self-assembled Cardin antimicrobial peptide amphiphiles (ACA-PA) with the sequence of C_{16}-V4K_4G(AKKARA)$_2$ to combat bacterial drug resistance [46]. ACA-PA forms spontaneous aggregates induced by hydrophobic collapse when the peptide concentration is above 45 μM. Structural experiments revealed that the amphiphilic Cardin antimicrobial peptide can fold into β-sheet secondary conformation and self-assemble into cylindrical supramolecular structures. TEM imaging revealed that the self-assembled structures of ACA-PA are nanorods with diameters in the range of 7–10 nm at the concentration of 1 mg/mL. 40 μM ACA-PA caused bacterial cytoplasmic leakage, local membrane disruption in gram-positive bacteria, and disorganization of gram-negative bacterial membrane. Thus, the nanoparticles formed by ACA-PA are potentially promising candidates to be used as antimicrobial agents [46]. To investigate the bactericidal effects of the ACA-PA-based nanomaterial, a viable colony count assay and the live/dead staining assay were conducted against gram-positive and gram-negative bacteria, *S. aureus*, MRSA, *E. coli*, and MDR *E. coli*. At concentrations higher than 80 μM, the ACA-PA nanorods possessed significant toxicity against all the bacteria and decreased colony-forming units for both *S. aureus* and MRSA by two logs. As for gram-negative *E. coli* and MDR *E. coli*, ACA-PA nanorods had potent bactericidal effects. Drug-resistant bacterial strains were exposed to ACA-PA at concentrations below (40 μM) and above (80 μM) the CMC, and then were visualized by TEM to reveal the damage in bacterial cell envelopes caused by the ACA-PA treatment. After the treatment with 40 μM of ACA-PA, the peptidoglycan layer of MRSA was partially damaged and the cytoplasmic membrane was no longer attached to the outer membrane, resulting in cytoplasmic leakage. By using 80 μM of ACA-PA, the disintegration of the bacterial cell wall became apparent in TEM images, which is indicative of local disruption of the cell membrane and complete leakage of the cytoplasm.

Self-assembled peptide-based nanomaterials can also be used as drug delivery carriers against bacteria. For example, the resistance of bacteria to the relatively nontoxic first-line antibiotics makes it necessary to treat infections with some powerful antibiotics. However, these antibiotics are kept in reserve due to their toxicity, which can lead to symptoms worse than the infection itself, such as fever, kidney damage, thrombophlebitis, and red man syndrome. Researchers are trying to find new and safer antibiotics, which can be delivered to the infected tissues and organs to increase drug potency and reduce their side effects. In order to achieve this purpose, one approach is to package the drug into nanoparticles, which prolongs the

half-life time of the payload antibiotic. Another strategy is targeting an antibiotic to bacteria in an infected tissue. Nanoparticle delivery with specific targeting drugs is an effective means of improving drug delivery. Ruoslahti and coworkers designed and synthesized a kind of vancomycin-loaded nanoparticles with the cyclic 9-amino-acid peptide CARG peptide, cyclo(CARGGLKSC). This designed drug increases the antibacterial activity of nanoparticles in *S. aureus*-infected tissues and reduces the side effects (Fig. 7.18) [47]. The nanoparticles have a porous silicon core which

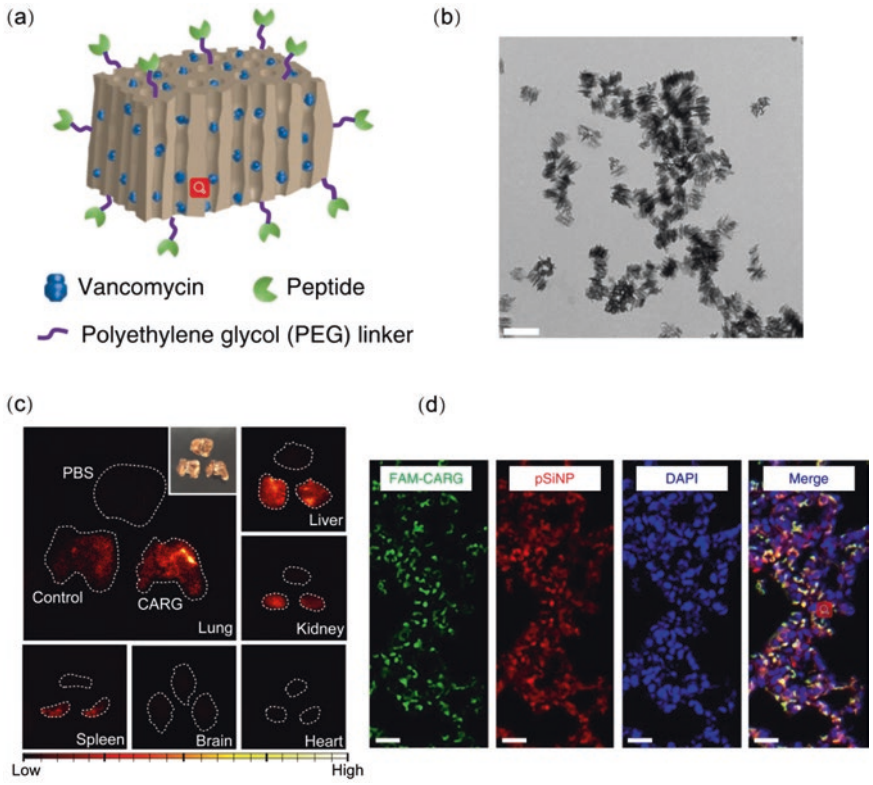

Fig. 7.18 Targeted drugs delivery to *S. aureus*-infected lungs in vivo. (**a**) A schematic illustration of the therapeutic nanoparticle system. (**b**) TEM image of vancomycin-loaded pSiNP (the scale bar is 200 nm). (**c**) Time-gated luminescence images of pSiNPs in mice after 1 h of circulation ($\lambda_e = 500$ nm). Nanoparticles were intravenously injected into infected mice 24 h post intratracheal administration of *S. aureus*. White dashed line indicates the outer boundary of each organ. The pSiNPs grafted with polyethylene glycol only (no targeting peptide) were the control nanoparticles; negative control: 50 μL corresponding volume of PBS was injected to mice intravenously. The inset is the white light photograph of lung tissues corresponding to the time-gated luminescence image. (**d**) Confocal fluorescence microscope images of the infected lung tissue of mice with CARG-pSiNPs. Green, red, and blue represent the CARG peptide labeled with FAM, intrinsic photoluminescence of pSiNPs, and DAPI nuclear stain, respectively (scale bars are 20 μm). Reproduced from [47]

provides high loading capacity for drugs and easily modified surface to accommodate targeting groups. The cyclic 9-amino-acid peptide cyclo(CARGGLKSC) that specifically binds to *S. aureus*-infected tissues was selected via a phage display peptide library screen in the mice with *S. aureus*-induced lung infections. In vivo and in vitro study results revealed that cyclo(CARGGLKSC) binds specifically to *S. aureus* bacteria and selectively accumulates in *S. aureus*-infected lungs and skin of mice. Thus, it significantly enhanced the local accumulation of intravenously injected vancomycin-loaded porous silicon nanoparticles to the infected area. Compared with vancomycin nanoparticles not labeled with cyclo(CARGGLKSC) and free vancomycin, these targeted nanoparticles more effectively suppressed staphylococcal infections in vivo. This development indicated a powerful and unbiased way to discover peptides that specifically accumulate in diseased tissues [47].

Another application of a peptide self-assembled nanomaterial against infection is the incorporation into pharmaceutical formulations that can continuously release hydrophobic and low-soluble antibiotics and provide a means of maintaining drug concentrations above the minimum inhibitory concentration for the pathogen. For example, ciprofloxacin is a gold standard for various topical applications, such as eye and skin infection. However, ciprofloxacin is sparingly soluble, and it is difficult to maintain dosing at a certain concentration. Hartley and coworkers reported the self-assembly of ciprofloxacin and a tripeptide (D-Leu-Phe-Phe) into supramolecular nanostructures, which were used in solving this solubility problem [48]. The soluble ciprofloxacin and the hydrophobic D-Leu-Phe-Phe can form supramolecular nanostructures that form macroscopic hydrogels at physiological pH (Fig. 7.19). The presence of non-covalent interactions between ciprofloxacin and the peptide hydrogel was confirmed by fluorescence spectroscopy and CD spectroscopy. Ciprofloxacin-loaded peptide hydrogel showed an antimicrobial efficacy against several bacteria, including *Escherichia coli*, *Staphylococcus aureus*, and *Klebsiella pneumonia*. No obvious cytotoxicity was found in lytic assays against human red blood cells or mouse fibroblast cell cultures. This work demonstrates the potential clinical applications of a peptide hydrogel as cost-effective wound dressings and novel antimicrobial formulations [48].

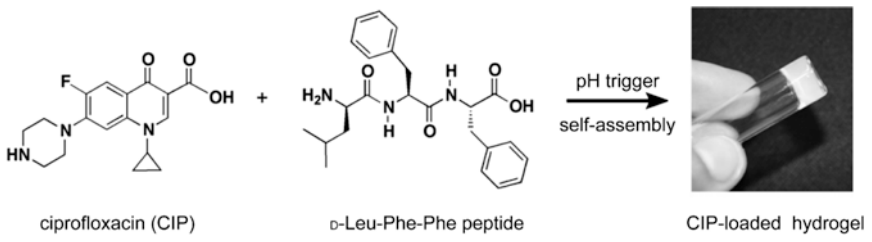

Fig. 7.19 Structures of ciprofloxacin (CIP) and peptide D-Leu-Phe-Phe that self-assemble into a hydrogel after being triggered by pH. Reprinted with permission from [48]. Copyright 2013 Elsevier

7.2.6 *Encapsulation of Peptide by Nanomaterials Against Bacteria*

Generation of nanomaterial delivery systems has been reported to be a promising strategy to improve peptide bioavailability. Nanomaterials can act as target-specific carriers to deliver therapeutic cargo for diagnosis and therapy, protect a peptide drug from proteolytic degradation, and alter the rapid peptide metabolism and elimination timescales in vivo [7–10]. Herein, we provide several recent examples demonstrating the applications of nanomaterials with encapsulated peptides in the context of treating bacterial infections.

Kwon and coworkers designed a bifunctional peptide that displays a killing domain (D-Asp-Lys-Lys) and a microbial *Pseudomonas* localization domain (a membrane-active peptide which is *Pseudomonas*-specific) and kills *Pseudomonas aeruginosa* at sub-micromolar concentrations [49]. Histological examinations of the lungs of mice treated with free peptide revealed that treatment resulted in bronchitis, sloughing of the bronchial epithelium, and interstitial pneumonitis; all of these symptoms developed in response to the toxicity of the antimicrobial peptide. When the bifunctional peptide was loaded into the pores of a biocompatible porous silicon nanoparticle (pSiNP) by electrostatic interactions and then dosed in mice, the peptide-pSiNP exhibited a better biodistribution and decreased the side effects of antimicrobial peptide in vivo. The encapsulation of the peptide by the nanoparticle significantly weakened the damage to the lung tissue. To examine the utility of peptide-pSiNP in vivo, this co-assembly material was delivered to the lungs of mice and tested for its potency against *P. aeruginosa* infection. The treatment of a lung infection model of *P. aeruginosa* (2×10^5 colony-forming unit (CFU) per mouse) with peptide-pSiNP (a mouse was given two doses of 1.5 nmol peptide and 30 μg porous silicon nanoparticle) resulted in an improved survival at 24-h post-infection from 10 to 20% (vehicle control) to 100%. To determine the effect of peptide nanoparticle on bacteria in vivo, mice were intratracheally instilled with 1×10^3 CFU *P. aeruginosa* per mouse to establish an infection model with near 100% 24-h survival and treated with peptide-pSiNPs. The utility of peptide-loaded nanoparticles markedly reduced the average bacterial number recovered from lungs from $1 \times 10^{5.2}$ CFU per lung (untreated mice) to $1 \times 10^{2.7}$ CFU per lung.

Other nanomaterials such as gold nanoparticles [9, 50] and graphene oxide [51] have also been shown to be efficient platforms to conjugate with antimicrobial peptides, increasing peptide proteolytic stability and decreasing peptide mammalian cell cytotoxicity. Rai et al. incorporated a cysteine residue to the C-terminus of an antimicrobial peptide, Cecropin-melittin, and covalently immobilized this peptide onto the surfaces of gold nanoparticles via Au-S bonds (Fig. 7.20) [50]. Cecropin-melittin modified gold nanoparticles at a concentration of 50 μg/mL exhibited high antimicrobial activity in human serum against gram-positive bacteria (*S. aureus*) and gram-negative bacteria (*E. coli*, *K. pneumoniae*, and *P. aeruginosa*). In addition, peptide-gold nanoparticles had higher resistance to enzymatic degradation than free peptides when they were treated with trypsin, *S. aureus* V8 protease, and human neutrophil elastase, respectively.

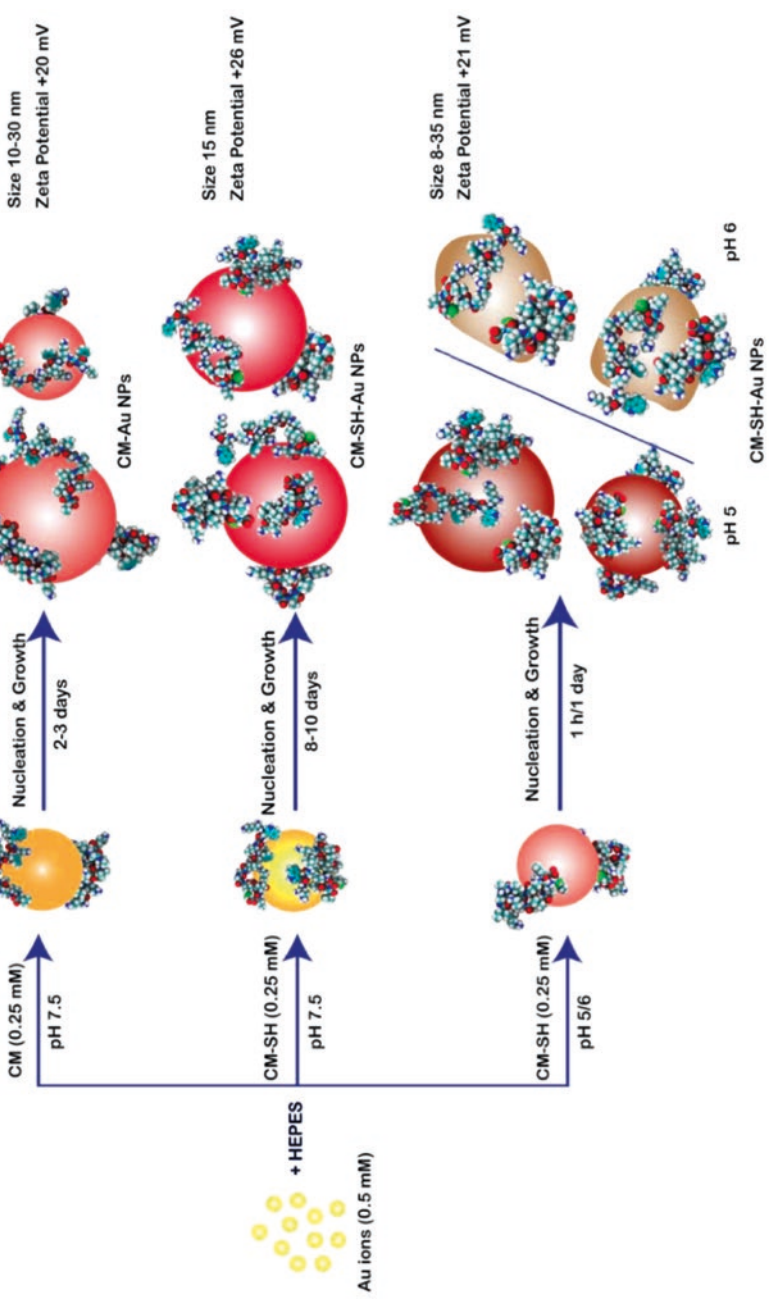

Fig. 7.20 Schematic illustration of Au nanoparticles synthesis in the presence of Cecropin-melittin (CM) peptides and CM-SH, under different experimental conditions. Reprinted with permission from [50]. Copyright 2016 Elsevier

Chen et al. non-covalently deposited an antimicrobial lipopeptide, surfactin, on the surfaces of dodecanethiol-capped gold nanodots via the hydrophobic interactions formed between the nonpolar tails of surfactin and dodecanethiol [9]. The minimal inhibitory concentration values of surfactin/dodecanethiol/gold nanodots against *E. coli*, *P. vulgaris*, MRSA, *S. aureus*, and *S. enteritidis* were much lower (less than 25 μM) than that of free surfactin (200–250 μM). Cytotoxicity evaluation using MCF-10A, NIH-3T3, and HMEC-1 cells and the hemolysis analyses using human red blood cells revealed superior biocompatibility of surfactin/dodecanethiol/gold nanodots relative to surfactin. To test the clinical applicability of this surfactin-gold nanodot material, histological analysis was carried out to evaluate the antibacterial ability in healing of skin wounds of rats exposed to MRSA. When compared to the untreated group, a greater migration for keratinocytes, higher fibroblast formation and collagen secretion, more blood vessels, and hair follicles were observed in the surfactin-gold nanodot-treated wound site relative to controls. Taken together, encapsulating peptides by nanomaterials has been demonstrated as a powerful strategy to improve the preclinical applications of antimicrobial peptides in the treatment of infections.

7.3 Development of Peptide Mimetic Materials with Antibacterial Activity

A key point that emerges from the progress described above is that diverse natural amino acid building blocks lie at the heart of the polypeptide assembly world. When appropriately coupled through amide linkages, these subunits direct folding into a particular type of secondary structure. The resulting structure provides a scaffold for the three-dimensional display of side chains. The spatial organization of side chains facilitates the non-covalent interactions between adjacent secondary structures to form both tertiary structure and quaternary structure, and then finally, a functional peptide assembly is achieved. In the past decade, increasing work has been devoted to exploring the diversity within the polypeptide backbone by using unnatural amino acids for molecular design. Alternative to the α-peptide scaffold, the β-peptide provides a new direction toward mimicking nature's molecular assemblies and antibacterial function.

7.3.1 β-Peptide: Molecular Structure and Conformational Stability

β-Peptides are oligomers composed of unnatural β-amino acids that mimic various aspects of the folding and organization of polypeptides. β-Amino acids contain an extra carbon in the backbone relative to α-amino acids (Fig. 7.21a). The

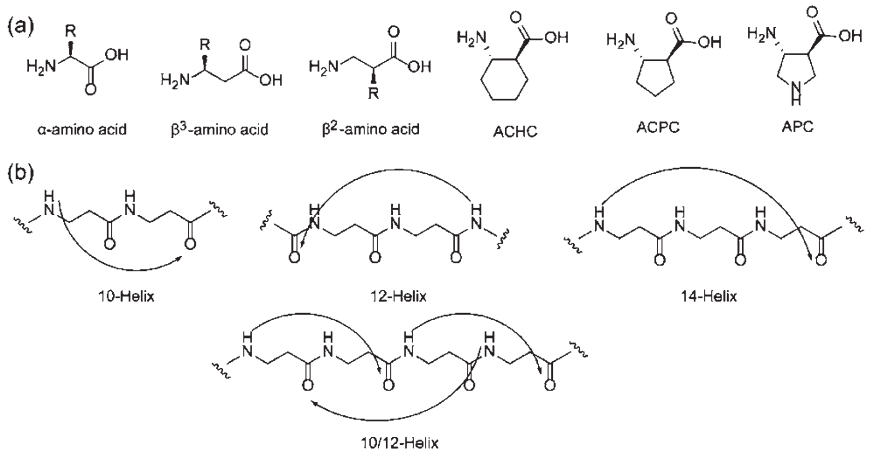

Fig. 7.21 (**a**) α- and β-amino acids. (**b**) Hydrogen-bonding patterns of β-peptide helices are shown with arrows

introduction of an additional carbon atom into the peptide backbone leads to an increase of a peptide's proteolytic stability [52]. Like α-peptides, hydrogen bonding between amino groups and carboxyl groups in neighboring regions of backbone folds β-peptide into specific secondary structures, including helices, sheets, and turns. Helices have been the most intensively studied.

The backbones of β-peptides are longer than those of peptides that consist of α-amino acids; thus β-peptides form different secondary structures (Fig. 7.21b) [52]. β-Peptides that consist exclusively of β^3-, β^2-, or cyclically constraint *trans*-2-aminocyclohexanecarboxylic acid (ACHC) residues form a 14-helix. The structure of the 14-helix is stabilized by hydrogen bonds between amides at position *n* and a main chain carbonyl group at position $n + 2$. Different from an α-helix, the 14-helix has a 3.6-residue repeat. Altering the cyclically constrained residue from 6-membered ring, ACHC, to a 5-membered ring residue, *trans*-2-aminocyclopentanecarboxylic acid (ACPC) or *trans*-3-aminopyrrolidine-4-carboxylic acid (APC), facilitates the formation of a 12-helix. β-Peptides composed entirely of a 4-membered ring constraint display a 10-helix secondary structure. β-Peptides composed of the repeated β^2- and β^3-residue units, such as poly(β^2-homoalanine-β^3-homoalanine), adopt a 10/12-helix conformation.

7.3.2 Intermolecular Interactions Encoded by β-Peptides

Understanding the origins of intermolecular interactions leading to self-assembly is one of the key challenges underlying the rational design of novel nanostructured functional materials. In particular, the association of nonpolar groups in water through "hydrophobic interactions" has been widely recognized as a key driving

force for nanoscale self-assembly [53]. Hydrophobic interactions are water-mediated interactions between nonpolar molecules or surfaces [53]. These interactions provide a principal driving force for polypeptide folding, protein assembly, and biomacromolecule-ligand association in aqueous solution and at aqueous interfaces. Hydrophobic interactions are influenced by other non-covalent interactions that are mediated by adjacent functional groups, engendering highly specific tertiary and quaternary structures observed among proteins and other biomolecular structures and complexes. To date, simulations rather than experiments have been used to explore the ways in which nanoscale chemical heterogeneity impacts hydrophobic interactions [53]. Experimental strategies for addressing this challenging topic are necessary in order to test computationally derived predictions. Contemporary simulations often ignore key features of real molecules, such as the polarizability of atoms and dissociation of water, which sharpens the need for incisive experimental approaches.

In order to study the influence of nanoscale chemical heterogeneity on hydrophobic interactions, Ma and coworkers reported single-molecule force measurements performed using a β-peptide that adopted a rigid and predictable conformation [54]. Relatively short β-peptides (7–12 residues) in which at least 30% of the residues contain the cyclohexyl constraint are fully helical in aqueous solution. The β-peptide helical structures display well-defined nano-domains of hydrophobic and hydrophilic groups, allowing for precise tailoring of the three-dimensional presentation of chemical groups via specification of the β-amino acid sequence. β-Peptides provide a rigid platform to mimic chemical heterogeneity that is more in tune with realistic biological systems. The experimental system was based on β-peptides that fold into globally amphiphilic (GA) helices (Fig. 7.22a) [54]. These helices contain 14-atom hydrogen-bonded rings, each with about three residues per turn. One side of the helix displayed an array of six cyclohexyl side chains, introduced as ACHC residues, which constituted a nonpolar domain ~1 nm^2 in size. In addition to providing a nonpolar domain, the ACHC residues strongly preorganize the β-peptide backbone for 14-helical folding. The opposing face of the helix presented three cationic side chains, from either β^3-homolysine (β^3-hLys) or β^3-homoarginine (β^3-hArg), ~1 nm from the nonpolar domain. The sequences and the predicted globally amphiphilic conformations, GA-KKK and GA-RRR, are shown in Fig. 7.22. Each β-peptide was immobilized onto a surface, and the influence of the cationic groups on hydrophobic adhesion was quantified between the ACHC-rich face of single oligopeptides and the tip of an atomic force microscope (AFM) that was made nonpolar by a coating with gold and adsorbing a monolayer of dodecanethiol (Fig. 7.22b). Hydrophobic interactions were quantified by comparing adhesive forces measured between a single surface-immobilized β-peptide molecule and a nonpolar AFM tip in either aqueous triethylammonium (TEA) buffer or TEA with 60 vol% MeOH (Fig. 7.22c). 85% of hydrophobic interactions are eliminated by 60 vol% MeOH, but its use does not measurably change screened Coulomb (electrical double layer) interactions. Accordingly, pull-off forces measured in the 60 vol% MeOH/40 vol% 10 mM TEA buffer are identified as being van der Waals interactions and electrostatic interactions in origin. Short β-peptides containing more than 30% ACHC

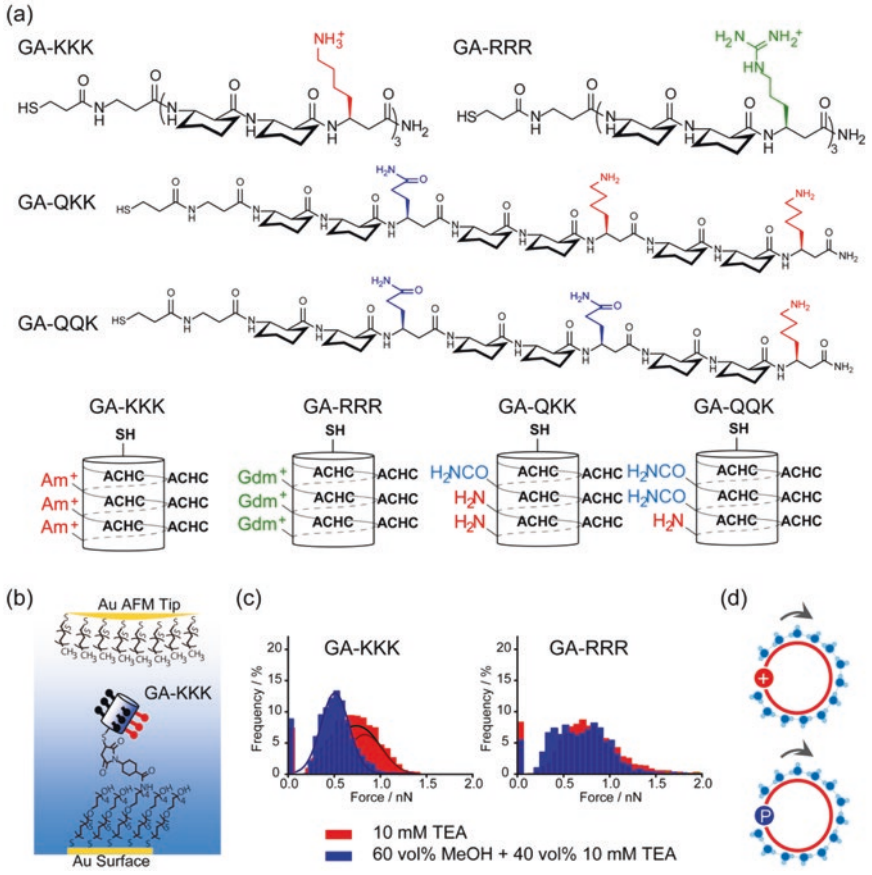

Fig. 7.22 (**a**) Chemical structures and helical cartoons for the β-peptides. (**b**) Schematic illustration of single-molecule force measurements with β-peptides. (**c**) Histograms of adhesion forces measured between an alkyl-terminated AFM tip and immobilized GA-KKK (left) or GA-RRR (right) peptides in either 10 mM TEA, pH 7 (red), or 60 vol% MeOH, pH 7 containing TEA solution (blue). (**d**) Influence of charged and polar side chains on the interfacial water structures of globally amphiphilic β-peptides. The solid red disk represents the side chains of β^3-homolysine residues. The blue disk with a white "P" sign represents the side chains of β^3-homoglutamine residues. Light blue spheres represent the interfacial water molecules [54, 55]. (**a**), (**c**), and (**d**) reprinted with permission from [55]. Copyright 2017 American Chemical Society

exhibit stable 14-helical conformations in aqueous solution and aqueous methanol, which allows for identification of hydrophobic interactions via addition of methanol. Conventional peptides, comprised of α-amino acid residues, lack sufficient α-helix stability to allow this experimental design. For the lysine-containing β-peptides (GA-KKK), adhesive interactions with the AFM tip are dependent on pH when measured in aqueous TEA. The addition of 60 vol% methanol causes the distribution of adhesive interactions. To quantify the hydrophobic component of the adhesive interactions between GA-KKK and the nonpolar AFM tip, a single

Gaussian function was fitted to each histogram measured in the presence of methanol (non-hydrophobic interactions). Two Gaussian functions were used to fit the histograms measured in aqueous TEA, one of which coincided with the Gaussian function fit in the presence of methanol (Fig. 7.22c). The forces described by the Gaussian function in aqueous TEA that were eliminated by the addition of methanol are the hydrophobic interactions between the ACHC domain of GA-KKK and the AFM tip. The methanol-independent forces arise from non-hydrophobic interactions, such as direct interactions of the β^3-hLys residues of GA-KKK with the AFM tip. This analysis led to the conclusion that the charge of the β^3-hLys side chain amino groups strengthens hydrophobic interactions between the nonpolar domain of GA-KKK and the AFM tip. The mean pull-off forces arising from hydrophobic interactions between the nonpolar ACHC-rich domains of GA-KKK and the alkyl-terminated AFM tip were determined to be 0.61 ± 0.04 nN at pH 10.5, and increased to 1.07 ± 0.01 nN at pH 7. To explore the role of the cationic residues in modulating the hydrophobic adhesion mediated by the nonpolar domains of the β-peptide, the β^3-hLys residues were substituted by β^3-hArg residues to generate GA-RRR. In striking contrast to the behavior of GA-KKK, adhesive interactions measured between GA-RRR and the AFM tip were largely unaffected by the addition of methanol (Fig. 7.22c). These observations suggest that the adhesive interactions measured with GA-Arg are not of hydrophobic origin. As a summary, when using GA-KKK, protonation of the side chains of β^3-hLys was measured to increase the strength of the hydrophobic adhesion between the AFM tip and the ACHC-rich domain. As a contrast, results of GA-RRR study showed that the guanidinium-containing β^3-hArg side chains eliminated measurable hydrophobic interactions. This observation indicates that charged groups immobilized within ~1 nm of a nonpolar domain can modulate the strength of the hydrophobic interaction mediated by the domain, and that the structure of the cationic group (ammonium vs. guanidinium) rather than net charge was crucial to the mode of action.

It is proposed that a possible mechanism by which proximal charged groups might influence hydrophobic interactions is that perturbations to the structure of interfacial water near charged groups on one face of the helix propagate, via water-water interactions (e.g., hydrogen bonding), from the site of the immobilized charges to the water adjacent to the nonpolar domain (Fig. 7.22d). These perturbations may include local fluctuations in the density of water. If this mechanism is dominated by the propagation of perturbations to solvent structure, immobilized polar but non-ionic groups might also modulate hydrophobic interactions in a group-specific manner (Fig. 7.22d). To test this hypothesis, AFM measurements with GA-QKK and GA-QQK were carried out to monitor the influence of replacing β^3-hLys residues in GA-KKK with β^3-homoglutamine (β^3-hGln or Q) residues on the hydrophobic interactions of globally amphiphilic β-peptides (Fig. 7.22a) [55]. The adhesive forces generated by GA-QKK and GA-QQK in aqueous TEA and then in 60 vol% MeOH in 40 vol% TEA were measured using the methodology described above for GA-KKK. For GA-QKK, the mean pull-off force in 60 vol% MeOH was 0.30 ± 0.17 nN at pH 10.5 and increased to 0.37 ± 0.01 nN at pH 7, whereas the hydrophobic force was 0.54 ± 0.01 nN at pH 10.5 and increased to

0.73 ± 0.03 nN at pH 7. When an additional β^3-hLys was further substituted by β^3-hGln, to generate GA-QQK, the adhesion forces mediated by a single GA-QQK molecule were measured to be the same in 60 vol% MeOH and aqueous TEA. This result indicates that GA-QQK does not generate a measurable hydrophobic force. At pH 10.5, where the degree of protonation of the K side chain is low, hydrophobic adhesive interactions mediated by GA-KKK were measured to be 0.61 ± 0.04 nN, by GA-QKK to be 0.54 ± 0.01 nN, and by GA-QQK to be 0 ± 0.01 nN. This finding suggests that replacing an amine group (β^3-hLys side chain) with a primary amide group (β^3-hGln side chain) weakens the hydrophobic interaction generated by the six cyclohexyl side chains. The differential impact of primary amine vs. primary amide on hydrophobic interactions of neighboring nonpolar surfaces reflects changes in the structure of water in the vicinity of the peptide, which in turn is influenced by hydrogen bonding and van der Waals interactions between the water and polar groups on the peptide side chains. The permanent dipole of the amine group is 1.31 D (methylamine in gas) and the amide group is 3.76 D (acetamide in gas). The geometries of the two groups are different because the amine nitrogen is sp^3-hybridized, while the amide nitrogen atom is sp^2-hybridized. Primary amine and primary amide groups have distinct abilities to form hydrogen bonds with the surrounding water molecules. The hydration free energy of acetamide (−39.9 kJ/mol) is larger relative to the *n*-butylamine (−18.0 kJ/mol). The hydration free energies are different because a primary amide likely forms more hydrogen bonds than a primary amine to water. In particular, the primary amide N-H are better hydrogen bond donors than primary amine N-H. The resonance stabilization of amides results in a partial negative charge on O and partial positive charge on N. This interaction enhances the proton accepting ability of O and makes the N-H group a stronger hydrogen bond donor (the free energy of HCOHN-H…OH_2 is −28.4 kJ/mol) than the N-H group of an amine (the free energy of H_2N-H…OH_2 is −6.3 kJ/mol). Overall, compared to an amine group, an amide group is expected to possess a stronger ability to form hydrogen bonds with nearby water, which will decrease the interfacial energy and perturb the structure of water adjacent to the nonpolar domain. It highlights the nonadditive nature of the interactions mediated by water at chemically heterogeneous surfaces.

The study mentioned above reveals the correlation between the hydration free energy of polar group and the impact of polar group on hydrophobic interactions of neighboring nonpolar surfaces. It provides a possible mechanism to interpret the influence of proximal cation identity on hydrophobic interactions. Specifically, the differential impacts of β^3-hLys versus β^3-hArg on peptide hydrophobicity reflect changes in the structure of water in the vicinity of the peptide, which is influenced by hydrogen bonding and van der Waals interactions between the water and charged groups on the peptide side chains in turn. Chemical properties of ammonium (β^3-hLys) and guanidinium (β^3-hArg) ions are distinct. The geometries of the two ions are distinct because the ammonium nitrogen is sp^3-hybridized while the guanidinium nitrogen atom is sp^2-hybridized. Ammonium and guanidinium ions have different abilities to form hydrogen bonds with surrounding water molecules. The hydration free energy of guanidinium (−583 kJ/mol) is larger relative to ammonium

(−285 kJ/mol). The hydration free energies are different because a guanidinium group likely forms more hydrogen bonds to water than an ammonium group because guanidinium contains more hydrogen bond donors than ammonium. Overall, when compared to ammonium (β^3-hLys side chain), a guanidinium group (β^3-hArg side chain) is expected to possess a stronger ability to form hydrogen bonds with nearby water, which will decrease the interfacial energy and perturb the structure of water adjacent to the nonpolar domain of peptide. This finding that the effective hydrophobicity of a nonpolar surface can be strongly influenced by the identity of proximal cationic groups, rather than simply by the presence of proximal charge, raises important questions about the impact of the identity of a charged group on noncovalent associations involving biomolecules. For example, mutation of lysine to arginine, or vice versa, is generally regarded as a conservative change in a protein. These results suggest that this assumption may require re-evaluation. If differences between the effects of proximal guanidinium and ammonium groups on hydrophobicity are mediated by cation-water hydrogen bonding, then N-methylation of lysine or arginine side chains, a common form of post-translational modification, may have previously unanticipated consequences on protein interactions. N-methylation of either side chain influences hydrogen bond donor capacity without altering net charge at neutral pH. These prospects should motivate future studies.

7.3.3 β-Peptide: Hierarchic Assemblies and Functional Properties

The well-defined three-dimensional structure of the robust β-peptide helix provides a platform to display a wide array of functional properties. Past studies have demonstrated that two- and three-dimensional hierarchical self-assembly and functionalities can be accessed through subtle changes in the presentation of chemical groups on the periphery of the β-peptide 14-helix, which is controlled by the β-peptide linear sequence.

To create unnatural β-peptides that adopt discrete quaternary structures, Raguse and coworkers designed a series of amphiphilic β-peptides containing ACHC and β^3-hLys residues [56]. Cyclic constraints in sequence promote the formation of 14-helix. Thus, the β-peptide helix has all three β^3-hLys side chains aligned on one side of the helix and the six cyclohexyl rings defining a hydrophobic helical face (Fig. 7.23a). The hydrophobic interactions displayed by the hydrophobic helical face drive self-assembly of β-peptides in bulk solution. A β^3-homotyrosine (β^3-hTyr) was put at the N-terminus to facilitate peptide concentration determination. NMR was used to interrogate β-peptide aggregation status in solution. At a concentration below 1.4 mM in 100 mM CD_3CO_2H/CD_3CO_2Na, 9:1 H_2O:D_2O at pH 3.8, the β-peptide displayed sharp NMR lines, indicating that the β-peptides remained in monomeric form at low concentration. As peptide concentrations in aqueous solutions were increased, the NMR peaks of the β-peptide solution broadened and coalesced due to the formation of peptide aggregates. The presence of β-peptide

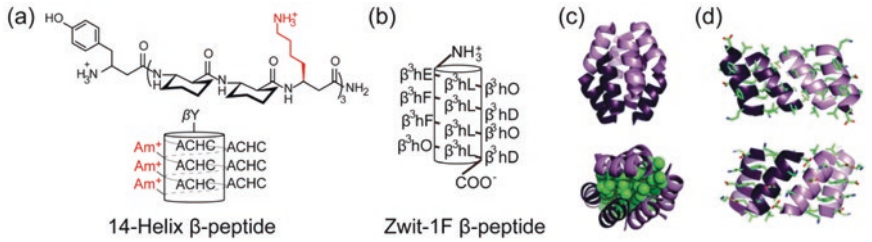

Fig. 7.23 (**a**) Chemical structure and helical cartoon for globally amphiphilic β-peptide. (**b**) Helical presentation for β-peptide Zwit-1F. (**c**) Ribbon diagram of the Zwit-1F octamer (top). Space-filling rendering of β^3-homoleucine side chains in green illustrates the well-packed hydrophobic core (bottom). (**d**) Interior (top) and exterior (bottom) views of each half show the hydrophobic and electrostatic interactions of the Zwit-1F assembly. (**c**) and (**d**) reprinted with permission from [58]. Copyright 2007 American Chemical Society

aggregates in solution was confirmed by using analytical ultracentrifugation (AUC) measurement. AUC studies were performed with the β-peptides at different concentrations in aqueous 10 mM Tris, pH 8.0, at several rotor speeds ranging from 35 to 60 krpm. Through AUC analysis, the amphiphilic β-peptide was observed to be monomeric at concentrations of 0.3 and 0.6 mM in 10 mM Tris, pH 8.0, but the radial distance spectra indicated that at least one aggregated state coexisted with the monomer when concentration was above 0.6 mM. To understand the aggregation states of the β-peptide in solution, the aggregation number of the peptide assemblies was calculated. According to the monomer/n-mer equilibrium model, 30–40% of the β-peptide was estimated to be hexameric at 1.7 mM. This finding led to the discovery that the β-peptides self-associated into a helix bundle quaternary structure, in which multiple helices associate with their long axes approximately aligned. Later, Pomerantz and coworkers identified a distinctive CD signature for self-assembled 14-helical β-peptides [57]. They found that the self-assembly of 14-helical β-peptides induces a diagnostic change in CD signature relative to monomeric 14-helices. Specifically, monomeric β-peptide 14-helices displayed a distinct CD minimum at 214 nm. Self-assembly of 14-helices leads to a shift in CD minimum from 214 nm to 205 nm. The onset of assembly is indicated by $[\theta]_{205}/[\theta]_{214} > 0.7$.

To investigate the structure of a β-peptide bundle, Daniels and coworkers designed a β-dodecapeptide (Zwit-1F) that self-assembles into a highly thermostable β-peptide octamer in aqueous solution and determined its structure by using X-ray crystallography (Fig. 7.23b) [58, 59]. Zwit-1F, composed of β^3-amino acids, favors a 14-helix secondary structure. Residues along one helical face are exclusively nonpolar residues (β^3-homoleucine, β^3-hLeu), providing a source of hydrophobic attractions for the self-association of β-peptides. This hydrophobic core is flanked by positively charged residues (β^3-homoornithine, β^3-hO) and negatively charged residues (β^3-homoaspartic acid, β^3-hD; β^3-homoglutamic acid, β^3-hE). Coulombic interactions generated by the complementary charges across the interface formed between different Zwit-1F helices can modulate assembly stability,

pairing preference, and helix orientation. At a concentration higher than 50 μM in phosphate buffer at pH 7.1, Zwit-1F peptide displayed a CD minimum at 205 nm, which indicates adoption of 14-helix bundle structure. To define the assembly state of Zwit-1F and detail the interactions within the assembly, its structure was determined by X-ray crystallography. Crystallographic analysis revealed that the Zwit-1F peptides assembled into what was defined as a β-peptide octamer model. The Zwit-1F octamer contains two pairs of tetrameric peptides, each composed of four 14 helices cupped at approximately a 90° angle to each other. The two halves of each tetramer are composed of symmetry-equivalent parallel dimers oriented in an antiparallel way. The 14-helical interfaces display association of β^3-hLeu faces, generating a solvent-excluded hydrophobic core in the octameric structure of Zwit-1F. Additionally, extensive inter-helical electrostatic interactions define the homo-oligomerization of Zwit-1F.

Supramolecular quaternary structures achieved by β-peptides encompass a set of novel three-dimensional hierarchical self-assembly materials with operational functionality. Pomerantz and coworkers found that globally amphiphilic β-peptides form liquid crystalline (LC) phases in water at β-peptide concentrations in the tens of mM range [60]. Polarized optical microscopy was used to monitor the formation of LC phases based on the observation of birefringence. To characterize the nanostructures of β-peptides that form in aqueous solutions, Cryo-EM was used to identify two different types of nanostructures, nanofibers, and globular aggregates. The nanofibers formed from the amphiphilic β-peptides were at least hundreds of nanometers in length and 10 nm in diameter. The high aspect ratio of nanofibers seems to be consistent with the length of mesogen required for LC phase formation. In contrast, globular aggregates were in the tens of nm in diameter and incapable of forming LC phases in water. Pomerantz and coworkers suggested that there is a concentration-dependent equilibrium between the two distinct types of nanostructures. At low β-peptide concentrations, the equilibrium favored formation of globular aggregates. Increasing the concentration of the β-peptide led to the coexistence of globular aggregates and nanofibers. At sufficiently high concentrations, nanofibers were the dominant aggregate form. Small bundles of β-peptides were expected to stack end-to-end forming micrometer-long nanofibers, and β-peptides were shown to form a dense, ordered nanofiber network in solution. Together, this study demonstrated that β-peptide hierarchical self-assembly can generate many types of aggregation.

Great progress has been made in the last decade toward the generation of protein-like architectures, including both secondary and quaternary structures with unnatural backbones. Biological activity has been achieved based on the formation of specific foldamer secondary structure. For example, inspired by the amphiphilic, helical, and cationic properties of α-helical host defense α-peptides, important progress has been made toward finding therapeutic use of 14-helix β-peptides against bacteria that are resistant to conventional antibiotics. Raguse and coworkers designed two series of cationic 9- and 10-residue β-peptides which form flexible amphiphilic 14-helices with analogs that have been rigidified by incorporation of the cyclohexyl-constrained ACHC residues [61]. By measuring the minimal

inhibitory concentration against gram-positive (*Bacillus subtilis*, *Staphylococcus aureus*, and *Enterococcus faecium*) and gram-negative (*E. coli*) bacteria, these β-peptides were found to possess antimicrobial activity comparable to or more potent than that of the conventional host defense α-peptides, melittin and magainin II amide [61]. Of particular significance, the biological activity of the β-peptides was specific for bacteria relative to mammalian cells. This selectivity profile was hypothesized to be dependent on the amphiphilic nature of the β-peptides, as globally amphiphilic β-peptides displayed low hemolytic activity at the corresponding bacterial minimum inhibitory concentrations, while non-globally amphiphilic β-peptides possessed antimicrobial activity at high concentrations also associated with high hemolytic activity. The mechanism of β-peptide antimicrobial activity is hypothesized to involve cell membrane disruption: cationic charge directs the peptides to anionic bacterial membranes, and hydrophobic side chains interact with the core of the lipid bilayer, ultimately destroying the barrier function of the membrane. Different from α-helical host defense peptides whose antibacterial activity decreases with increased α-helical stabilization, the antimicrobial activity of β-peptides is proposed to be independent of 14-helix propensity. ACHC-rich β-peptides were also reported to function as antifungal agents under conditions that render host defense α-peptides inactive against fungal pathogens. Karlsson and coworkers found that the β-peptide (ACHC-β^3-hVal-β^3-hLys)$_3$ displays antifungal activity against *Candida albicans* with a MIC at 17 μg/mL, which is significantly lower than that of conventional host defense peptide magainin (>128 μg/mL) [62].

β-Peptides bearing guanidinium groups in their side chains have been shown to mimic the cell penetration behavior of arginine-rich peptides, such as TAT peptides. TAT peptides are a set of peptides derived from the anti-human immunodeficiency virus (HIV) tat protein and possesses the ability to inhibit virus entry. For instance, one TAT peptide, GRKKRRQRRR, blocks HSV-1 infection at the entry step in cell culture with a 50% effective concentration (EC_{50}) of 1 μM. These findings indicated that β-peptides could be engineered to display antiviral activity against herpes simplex virus type 1 (HSV-1) infection. Akkarawongsa and coworkers designed a 14-helix β-peptide, β^3-hTyr-(ACHC-β^3-hArg-β^3-hArg)$_3$, and determined the inhibition of virus infection by the β-peptide [63]. Recombinant HSV-1 KOS mutant hrR3 virus was employed as a model system. HSV-1 hrR3 virus expresses a reporter β-galactosidase after the virus has entered the cell and released its genome to the nucleus, where transcription is activated. Thus, it allows the determination of virus infectivity by measuring the expression of β-galactosidase in cell. To determine whether the β-peptide was efficient at preventing HSV-1 infection, the β-peptide was added into Vero and HK320 mammalian cells before, during, and after HSV infection. The result demonstrates that β-peptide β^3-hTyr-(ACHC-β^3-hArg-β^3-hArg)$_3$ blocked HSV-1 infection at the postattachment entry step in cell culture (EC_{50} = 3 μM). This result suggests the potential use of cationic β-peptides as antiviral agents. To test whether the β-peptide inactivates virus, recombinant hrR3 virus was incubated with the β-peptides for a time course of 1 h and diluted 1000-fold into cell culture medium supplemented with β-peptide-free serum. To quantify the remaining infectious virus in cell cultures, the expression of β-galactosidase was

measured. The β-peptide was found to be incapable of inactivating virions in solution. Previous studies with TAT peptides revealed that they bind to sialic acids of HSV-1 glycoproteins, which in turn results in the disability of HSV-1 entry. Thus, as a mimic of TAT peptides, the underlying mechanism of these β-peptides at preventing virus infection might be related to its interactions with sialic acids [63].

7.3.4 Nylon-3 Polymers Against Pathogens

We have reviewed the structures and biological activities of β-peptides, which are oligomers composed of β-amino acids that mimic polypeptides. Next, we turn to introduce the progress of developing nylon-3 polymers. Nylon-3 polymers are polydisperse polymers whose subunit is a β-amino acid; the backbone of nylon-3 polymers thereby features periodic secondary amide groups [64]. These polymers resemble natural peptides and proteins, which are sequence-specific polymers composed of α-amino acid subunits. In comparison to natural peptides and proteins, nylon-3 polymers are faster and cheaper to synthesize and stable to hydrolysis by natural protease enzymes. The ability of nylon-3 polymers to form globally amphiphilic structures when in contact with biomembranes is believed to underlie their ability to compromise bacterial membrane barrier function and thus kill or inhibit the growth of prokaryotes. The remainder of this chapter will focus on the use of these polymers against human pathogenic bacteria.

For instance, Mowery and coworkers synthesized nylon-3 copolymers composed of cationic and hydrophobic subunits and tested their antibacterial activity [64]. Specifically, the nylon-3 copolymer, $MM_{60}CH_{40}$, which was composed of nonpolar six-membered ring side chains and positively charged ammonium-terminated side chains, was synthesized via the ring-opening copolymerization of two racemic β-lactams: 60% cationic subunits (monomethyl β-lactam, MM) and 40% hydrophobic subunits (*cis*-cyclohexyl β-lactam, CH) (Fig. 7.24a). The average molecular weight of $MM_{60}CH_{40}$ was determined by gel permeation chromatography (GPC) to be between 3000 and 3800 g/mol, which corresponds to an average polymer chain length of 16–20 subunits. The dispersity index of the copolymer was measured to be in the range of 1.3 to 1.7. The antibacterial activity of $MM_{60}CH_{40}$ was tested using standard broth dilution methods. The MIC of the MM60CH40 copolymer was 12.5 μg/mL (*E. faecium*), whereas the minimum hemolytic concentration (MHC) of $MM_{60}CH_{40}$ toward human red blood cells was measured to be 100 μg/mL. Parallel measurements were conducted with antimicrobial α-peptides, magainin 2 and cecropin A. For magainin 2, the MIC for *E. coli* was determined to be 100 μg/mL, and the MHC was higher than 400 μg/mL. For cecropin A, the MIC for *E. coli* was 0.78 μg/mL, and the MHC was higher than 400 μg/mL. Taken together, relative to the conventional antibacterial peptides, $MM_{60}CH_{40}$ possessed antimicrobial activity against a panel of bacteria at concentrations that were nontoxic to mammalian cells.

To understand the antibacterial mechanism of nylon-3 polymers, Lee and coworkers examined how nylon-3 copolymers induced membrane deformation on

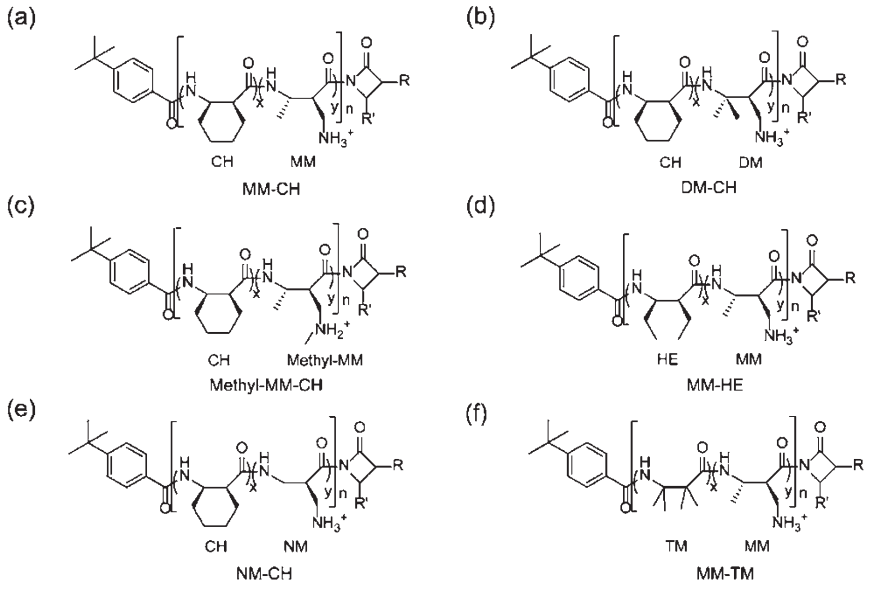

Fig. 7.24 Chemical structures for the nylon-3 polymers

synthetic vesicles and bacteria cell membranes [65]. They synthesized a nylon-3 copolymer, $DM_{50}CH_{50}$, by polymerizing cationic subunits (dimethyl β-lactam, DM) and hydrophobic CH subunits in a 1:1 molar ratio (Fig. 7.24b). The average molecular weight of $DM_{50}CH_{50}$ was determined to be 5129 g/mol, equivalent to 27 subunits. To test the impact of $DM_{50}CH_{50}$ on lipid membranes, vesicle dye leakage experiments were carried out. Unilamellar vesicles composed of DOPS/DOPE/DOPC = 20/60/20 were encapsulated with calcein dye in aqueous solution. Upon cleavage, calcein is released into solution, producing an increase in the fluorescence intensity at 510 nm. In the experiment, $DM_{50}CH_{50}$ was exposed to synthesized vesicles and observed to induce vesicle leakage. In parallel, a membrane permeability assay was performed with *E. coli* ML-35 strain to investigate the impact of DM50CH50 on a bacterial membrane. *E. coli* ML-35 strain possesses β-galactosidase activity but is lactose permease deficient. Hence, it is unable to uptake the lactose analog *o*-nitrophenyl-β-D-galactopyranoside (ONPG) unless it is permeabilized by membrane-disruptive agents. Upon membrane permeation, ONPG diffuses into the bacterial cell cytoplasm and is hydrolyzed by β-galactosidase to yield *o*-nitrophenol (ONP), which can be measured by absorbance at 405 nm. Increased absorbance was immediately observed after addition of a culture of *E. coli* ML-35, which suggests that $DM_{50}CH_{50}$ is a potent bacterial membrane permeabilization agent. The results from these two sets of independent systems, synthetic vesicles and *E. coli* ML-35 strain, demonstrate that the antibacterial mechanism of nylon-3 copolymer is correlated with its biomembrane disruption potency.

The studies mentioned above suggest that nylon-3 polymers represent a new class of promising antimicrobial agents that mimic the bacterial membrane disruption activity of natural host defense peptides. The general mechanism by which nylon-3 polymers lyse bacterial membranes first involves the coulombic attraction of the cationic side chains of nylon-3 polymers and the anionic surfaces of the bacterial cell, followed by the insertion of hydrophobic side chains of polymers into the nonpolar interior of the lipid membrane bilayer. The negative charge density of the external eukaryotic cell surfaces is lower than that of prokaryotic cell surfaces, which underlies the selectivity of nylon-3 polymer for targeting prokaryotic cells. The activity of conventional antimicrobial α-peptides is proposed to be that α-peptide forms a globally amphiphilic helical conformation upon the interactions with a biomembrane surface. In contrast, nylon-3 polymers are hypothesized to adopt specific but irregular conformations when in a micellar environment that results in global segregation of hydrophilic and lipophilic side chains. This hypothesis suggests that random sequences of cationic and nonpolar residues might be able to mimic host defense peptides [66].

To develop nylon-3 copolymers analogs with improved therapeutic properties, substantial efforts have been made to understand the structure-activity relationships in this polymer family. Several studies have focused on how varying structural parameters of nylon-3 polymers affects their minimum inhibitory concentrations against bacterial species and their hemolytic activity. Structural parameters such as nonpolar/cationic proportion, nonpolar subunit identity, length, cationic subunit identity, and end group on the antibacterial and hemolytic activities of nylon-3 copolymers have been evaluated for their impact on biological activity.

To explore the effects of nonpolar/cationic proportion on nylon-3 polymer activity, variations in the polymer composition were synthesized to include exclusively cationic MM subunits (MM_{100}), and cationic MM/nonpolar CH mixtures from $MM_{30}CH_{70}$ to $MM_{90}CH_{10}$. Homopolymer MM_{100} shows weak antibacterial activity toward *E. coli*, *S. aureus*, and *E. faecium* (MIC >50 μg/mL) and low hemolytic activity (MHC >1000 μg/mL) [66]. An increase in the proportion of nonpolar residue CH leads to improvement in antibacterial activity (MIC <50 μg/mL), until the nonpolar/cationic proportion reaches 50/50 ($MM_{50}CH_{50}$). Hemolytic activity remains very weak (MHC >800 μg/mL) until the nonpolar/cationic proportion reaches 40/60 ($MM_{60}CH_{40}$). A further decrease in the proportion of cationic residue MM results in an increase in hemolytic activity. Nylon-3 polymers composed of less than 50% cationic residues are hemolytic [66].

To explore the effects of nylon-3 polymer length on biological activity, a set of $MM_{63}CH_{37}$ copolymers with different chain lengths (10 to 60 subunits) were synthesized [66]. The MICs of $MM_{63}CH_{37}$ against *E. coli*, *B. subtilis*, *S. aureus*, and *E. faecium* are independent of the number of subunits in polymer chain, which reveals that nylon-3 antibacterial activity is not strongly affected by polymer chain length. In contrast to the trends in antibacterial activity, nylon-3 hemolytic activity is dependent on polymer chain length. Polymers containing an average of 10–30 subunits exhibit a very weak tendency to induce hemolysis, with MHC values in the vicinity of 1000 μg/mL. $MM_{63}CH_{37}$ copolymers with average chain lengths less than 30

subunits inhibited the growth of bacteria at much lower concentrations (1–100 μg/mL) than that required for human red blood cells (1000 μg/mL). The MHCs of polymers containing more than 30 subunits decreased to 1–10 μg/mL. $MM_{63}CH_{37}$ copolymers composed of more than 30 subunits were more hemolytic than their shorter analogs, with bacterial growth inhibitory concentration roughly equivalent to concentrations that induce hemolysis [66].

Substantial structure-activity relationship studies with nylon-3 polymers have been performed to evaluate the effects of residue side chain identity on the biological activity of these materials. The impact of primary amine versus secondary amine on the antibacterial activity has been examined via the direct comparison of the effects of two copolymers, $MM_{50}CH_{50}$ (number of subunits = 18) versus Methyl-$MM_{50}CH_{50}$ (number of subunits = 20) (Fig. 7.24c) [67]. $MM_{50}CH_{50}$ is cationic/nonpolar polymer presenting primary amine side chains, whereas Methyl-$MM_{50}CH_{50}$ incorporates *N*-methylated secondary amines. Relative to the nylon-3 polymer composed of primary amines, the addition of a methyl group to the side chain amines led to a decrease in antibacterial activity against a panel of bacteria (*E. coli*, *B. subtilis*, *S. aureus*), as well as a decrease in hemolytic activity. Charkraborty and coworkers demonstrated that differences in the antibacterial activities of nylon-3 polymers with cyclic versus acyclic side chains are correlated with their local backbone flexibilities [67]. The effects of cyclic versus acyclic nonpolar subunits were examined by comparing $MM_{60}CH_{40}$ (number of subunits = 15) versus $MM_{60}HE_{40}$ (number of subunits = 16) (Fig. 7.24d). Flexible polymer $MM_{60}HE_{40}$ containing acyclic nonpolar side chains displayed weak antibacterial property toward *E. coli* (MIC >200 μg/mL), relative to rigid polymer $MM_{60}CH_{40}$ containing the analogous cyclic subunit (MIC = 50 μg/mL). The impact of cyclic nonpolar side chain on the biological activities of nylon-3 polymers was further evaluated by varying the substitution pattern of the hydrophobic subunit. Mowery and coworkers synthesized copolymers containing cyclic nonpolar side chains of different ring sizes by copolymerizing CP (5-membered ring), CH (6-membered ring), CHp (7-membered ring), or CO (8-membered ring) to copolymerize with MM [66]. Comparison of these copolymers probed how variations in side chain size affected biological properties. They found that the hemolytic propensity of copolymer generally increases as the cycloalkyl ring size increases, but the correlation between cycloalkyl ring size and antibacterial activity is not clear.

The impact of end-group identity was explored by using a series of polymers containing N-terminal linear acyl units from acetyl (C_2) to octadecanoyl (C_{18}) [66]. These polymers contained 27–35 subunits and were prepared from a β-lactam mixture containing 63% MM and 37% CH. An increased terminal chain length from C_2 to C_{12} moderately decreased the MICs of copolymers against *E. coli*, *B. subtilis*, *S. aureus*, and *E. faecium.* Further increases in tail length from C_{12} to C_{18} significantly increased MIC values. This decrease in antibacterial efficacy is likely due to the increased aggregation tendency of polymers with the elongated nonpolar alkyl chain lengths. The hemolytic trends imply the N-terminal carbon tail enhances the ability of these polymers to lyse human red blood cells.

More recently, Liu and coworkers found that nylon-3 polymers displayed potent antifungal activity against *Candida albicans*, beyond strains *E. coli*, *B. subtilis*, and *S. aureus* [68]. *C. albicans* is part of our natural microflora and is the most common cause of fungal urinary tract infections. Cationic NM (no methyl β-lactam) was copolymerized with CH to obtain the nylon-3 polymers CH-NM (Fig. 7.24e). The antifungal activity against *C. albicans* increased as the proportion of CH decreased, and no detectable hemolytic activity. Cationic homopolymer displayed antifungal activity comparable to that of the most active CH-NM copolymers. Currently, therapeutic agents available to treat fungi are very limited and are plagued with rising levels of resistance. Thus, the discovery of new antifungal agents is a significant concern to clinicians responsible for treating invasive fungal infections. The finding that nylon-3 polymers are active against *C. albicans* represents an important prelude to new antifungal therapeutic strategy. To improve antifungal activity among nylon-3 materials, Rank and coworkers examined nylon-3 copolymers containing the nonpolar TM (tetramethyl β-lactam) subunit paired with either the MM or DM cationic unit with an average chain length of 20 subunits [69]. The MM-TM copolymer (Fig. 7.24f) showed activity against multiple species of *Cryptococcus* (*C. neoformans*, *C. gattii*) and Candida (*C. albicans*, *C. lusitaniae*) comparable to or more potent than clinically relevant drugs, amphotericin B and fluconazole. This polymer acted synergistically with azoles against different species of *Aspergillus* (*A. fumigatus*, *A. terreus*), including some azole-resistant strains. The activity of nylon-3 polymers against fungi from 18 pathogenic genera composed of 41 species and 72 isolates was further characterized [70]. Three types of nylon-3 polymers, DM-TM, MM-TM, and NM, show high efficacy against diverse fungi, including yeasts, dermatophytes, dimorphic fungi, molds, and even fungi that are intrinsically resistant to current antifungal drugs.

7.4 Conclusions

Self-assembly is an important process in nature. This chapter presents a brief overview of the diverse methods available to study self-assembled peptides, including the peptide amphiphiles and peptide mimetics that self-assemble into complex stable nanostructures. The examples introduced above include materials that elicit an array of biological activities in vitro and in vivo, and in this chapter, particular emphasis is placed on systems with antimicrobial activity. Despite promising activity, however, many hurdles still exist that limit the application of peptide-based nanomaterials in the fight against human pathogenic bacteria. The first is the safety of these nanomaterials. Toxic effects due to administration of these materials have been documented at the pulmonary, reproductive, cardiac, cutaneous, renal, and cellular levels. It is yet to be proven scientifically that the toxicity of nanomaterials was regulated by shape, size, area, and surface chemistry. Increased production and intentional or unintentional exposure to nanomaterials is likely to increase the probability of uncovering their adverse health effects. It is crucial that novel

nanomaterials be biologically characterized for their health hazards to ensure risk-free and sustainable implementation of nanotechnology. The second limitation is the controllability of the nanomaterial assembly. Relative to peptide-based self-assembled nanomaterials, DNA and RNA origami are more controllable in that individual molecules inherently assemble into intricate shapes and structures at the nanoscale. Improving the design method to build a well-ordered peptide self-assembled nanomaterial remains an important challenge at present. The clinical application of peptide self-assembled nanomaterials is also hindered by the poor druggability of peptides. Improvement of the oral availability and stability of peptide continues to be an area of future research.

References

1. A.A. Bahar, D. Ren, Antimicrobial peptides. Pharmaceuticals (Basel) **6**(12), 1543–1575 (2013)
2. M. Zasloff, Antimicrobial peptides of multicellular organisms: my perspective. Adv. Exp. Med. Biol. **1117**, 3–6 (2019)
3. M. Fernandez-Vidal et al., Folding amphipathic helices into membranes: amphiphilicity trumps hydrophobicity. J. Mol. Biol. **370**(3), 459–470 (2007)
4. K.A. Brogden, Antimicrobial peptides: pore formers or metabolic inhibitors in bacteria? Nat. Rev. Microbiol. **3**(3), 238–250 (2005)
5. K. Shimazaki et al., Properties of a heparin-binding peptide derived from bovine lactoferrin. J. Dairy Sci. **81**(11), 2841–2849 (1998)
6. L. Zhang, A. Rozek, R.E. Hancock, Interaction of cationic antimicrobial peptides with model membranes. J. Biol. Chem. **276**(38), 35714–35722 (2001)
7. D. Mandal, A. Nasrolahi Shirazi, K. Parang, Self-assembly of peptides to nanostructures. Org. Biomol. Chem. **12**(22), 3544–3561 (2014)
8. D.M. Raymond, B.L. Nilsson, Multicomponent peptide assemblies. Chem. Soc. Rev. **47**(10), 3659–3720 (2018)
9. W.-Y. Chen et al., Self-assembly of antimicrobial peptides on gold nanodots: against multidrug-resistant bacteria and wound-healing application. Adv. Funct. Mater. **25**(46), 7189–7199 (2015)
10. R.Y. Pelgrift, A.J. Friedman, Nanotechnology as a therapeutic tool to combat microbial resistance. Adv. Drug Deliv. Rev. **65**(13-14), 1803–1815 (2013)
11. R.G. Ellis-Behnke et al., Nano neuro knitting: peptide nanofiber scaffold for brain repair and axon regeneration with functional return of vision. Proc. Natl. Acad. Sci. U. S. A. **103**(13), 5054–5059 (2006)
12. T.C. Holmes et al., Extensive neurite outgrowth and active synapse formation on self-assembling peptide scaffolds. Proc. Natl. Acad. Sci. U. S. A. **97**(12), 6728–6733 (2000)
13. J. Kisiday et al., Self-assembling peptide hydrogel fosters chondrocyte extracellular matrix production and cell division: implications for cartilage tissue repair. Proc. Natl. Acad. Sci. U. S. A. **99**(15), 9996–10001 (2002)
14. S. Koutsopoulos et al., Controlled release of functional proteins through designer self-assembling peptide nanofiber hydrogel scaffold. Proc. Natl. Acad. Sci. U. S. A. **106**(12), 4623–4628 (2009)
15. J.S. Richardson, The anatomy and taxonomy of protein structure. Adv. Protein Chem. **34**, 167–339 (1981)
16. X. Guo et al., Solution structures and backbone dynamics of arsenate reductase from Bacillus subtilis: reversible conformational switch associated with arsenate reduction. J. Biol. Chem. **280**(47), 39601–39608 (2005)

17. C.J.C. Edwards-Gayle, I.W. Hamley, Self-assembly of bioactive peptides, peptide conjugates, and peptide mimetic materials. Org. Biomol. Chem. **15**(28), 5867–5876 (2017)
18. M.R. Ghadiri et al., Self-assembling organic nanotubes based on a cyclic peptide architecture. Nature **366**(6453), 324–327 (1993)
19. S. Fernandez-Lopez et al., Antibacterial agents based on the cyclic D,L-alpha-peptide architecture. Nature **412**(6845), 452–455 (2001)
20. H. Cui et al., Self-assembly of giant peptide nanobelts. Nano Lett. **9**(3), 945–951 (2009)
21. J. Wang et al., Dynamic self-assembly of surfactant-like peptides A(6)K and A(9)K. Soft Matter **5**(20), 3870–3878 (2009)
22. H. Xu et al., Hydrophobic-region-induced transitions in self-assembled peptide nanostructures. Langmuir **25**(7), 4115–4123 (2009)
23. G.A. Silva et al., Selective differentiation of neural progenitor cells by high-epitope density nanofibers. Science **303**(5662), 1352–1355 (2004)
24. I.W. Hamley et al., Self-assembly of a model amphiphilic oligopeptide incorporating an arginine headgroup. Soft Matter **9**(19), 4794–4801 (2013)
25. E.G. Bellomo et al., Stimuli-responsive polypeptide vesicles by conformation-specific assembly. Nat. Mater. **3**(4), 244–248 (2004)
26. M.R. Dreher et al., Temperature triggered self-assembly of polypeptides into multivalent spherical micelles. J. Am. Chem. Soc. **130**(2), 687–694 (2008)
27. M.I. Ivanova et al., Molecular basis for insulin fibril assembly. Proc. Natl. Acad. Sci. U. S. A. **106**(45), 18990–18995 (2009)
28. J.J. Wiltzius et al., Molecular mechanisms for protein-encoded inheritance. Nat. Struct. Mol. Biol. **16**(9), 973–978 (2009)
29. G.M. Clore, M.R. Starich, A.M. Gronenborn, Measurement of residual dipolar couplings of macromolecules aligned in the nematic phase of a colloidal suspension of rod-shaped viruses. J. Am. Chem. Soc. **120**(40), 10571–10572 (1998)
30. N. Tjandra, A. Bax, Direct measurement of distances and angles in biomolecules by NMR in a dilute liquid crystalline medium (vol 278, pg 1111, 1997). Science **278**(5344), 1697–1697 (1997)
31. G.M. Clore, J. Iwahara, Theory, practice, and applications of paramagnetic relaxation enhancement for the characterization of transient low-population states of biological macromolecules and their complexes. Chem. Rev. **109**(9), 4108–4139 (2009)
32. D.A. Middleton et al., Insights into the molecular architecture of a peptide nanotube using FTIR and solid-state NMR spectroscopic measurements on an aligned sample. Angew. Chem. Int. Ed. Engl. **52**(40), 10537–10540 (2013)
33. J. Frank, Averaging of low exposure electron-micrographs of non-periodic objects. Ultramicroscopy **1**(2), 159–162 (1975)
34. H. Shen et al., De novo design of self-assembling helical protein filaments. Science **362**(6415), 705–709 (2018)
35. X.J. Ma et al., Amyloid beta (1-42) folding multiplicity and single-molecule binding behavior studied with STM. J. Mol. Biol. **388**(4), 894–901 (2009)
36. X.B. Mao et al., Beta structure motifs of islet amyloid polypeptides identified through surface-mediated assemblies. Proc. Natl. Acad. Sci. U. S. A. **108**(49), 19605–19610 (2011)
37. X.B. Mao et al., Binding modes of Thioflavin T molecules to prion peptide assemblies identified by using scanning tunneling microscopy. ACS Chem. Nerosci. **2**(6), 281–287 (2011)
38. C.X. Wang et al., Determination of relative binding affinities of labeling molecules with amino acids by using scanning tunneling microscopy. Chem. Commun. **47**(38), 10638–10640 (2011)
39. C. Walsh, Molecular mechanisms that confer antibacterial drug resistance. Nature **406**(6797), 775–781 (2000)
40. D.H. Williams et al., An analysis of the origins of a cooperative binding energy of dimerization. Science **280**(5364), 711–714 (1998)
41. C. Ren et al., Interfacial self-assembly leads to formation of fluorescent nanoparticles for simultaneous bacterial detection and inhibition. Chem. Commun. (Camb.) **50**(26), 3473–3475 (2014)

42. L.L. Li et al., Pathological-condition-driven construction of supramolecular nanoassemblies for bacterial infection detection. Adv. Mater. **28**(2), 254–262 (2016)
43. C. Yang et al., Dual fluorescent- and isotopic-labelled self-assembling vancomycin for in vivo imaging of bacterial infections. Angew. Chem. Int. Ed. Engl. **56**(9), 2356–2360 (2017)
44. I. Acebron et al., The allosteric site for the nascent cell wall in penicillin-binding protein 2a: an Achilles' heel of methicillin-resistant Staphylococcus aureus. Curr. Med. Chem. **22**(14), 1678–1686 (2015)
45. M.T.G. Holden et al., Complete genomes of two clinical Staphylococcus aureus strains: evidence for the rapid evolution of virulence and drug resistance. Proc. Natl. Acad. Sci. U. S. A. **101**(26), 9786–9791 (2004)
46. R. Chang et al., Enhanced antibacterial properties of self-assembling peptide Amphiphiles functionalized with heparin-binding Cardin-motifs. ACS Appl. Mater. Interfaces **9**(27), 22350–22360 (2017)
47. S. Hussain et al., Antibiotic-loaded nanoparticles targeted to the site of infection enhance antibacterial efficacy. Nat. Biomed. Eng. **2**(2), 95–103 (2018)
48. S. Marchesan et al., Self-assembly of ciprofloxacin and a tripeptide into an antimicrobial nanostructured hydrogel. Biomaterials **34**(14), 3678–3687 (2013)
49. E.J. Kwon et al., Porous silicon nanoparticle delivery of tandem peptide anti-infectives for the treatment of Pseudomonas aeruginosa lung infections. Adv. Mater. **29**(35), 1701527 (2017)
50. A. Rai et al., One-step synthesis of high-density peptide-conjugated gold nanoparticles with antimicrobial efficacy in a systemic infection model. Biomaterials **85**, 99–110 (2016)
51. R. Kanchanapally et al., Antimicrobial peptide-conjugated graphene oxide membrane for efficient removal and effective killing of multiple drug resistant bacteria. RSC Adv. **5**(24), 18881–18887 (2015)
52. R.P. Cheng, S.H. Gellman, W.F. DeGrado, Beta-peptides: from structure to function. Chem. Rev. **101**(10), 3219–3232 (2001)
53. S. Garde, Hydrophobic interactions in context. Nature **517**(7534), 277–279 (2015)
54. C.D. Ma et al., Modulation of hydrophobic interactions by proximally immobilized ions. Nature **517**(7534), 347–350 (2015)
55. C. Wang et al., Nonadditive interactions mediated by water at chemically heterogeneous surfaces: nonionic polar groups and hydrophobic interactions. J. Am. Chem. Soc. **139**(51), 18536–18544 (2017)
56. T.L. Raguse et al., Toward beta-peptide tertiary structure: self-association of an amphiphilic 14-helix in aqueous solution. Org. Lett. **3**(24), 3963–3966 (2001)
57. W.C. Pomerantz et al., Distinctive circular dichroism signature for 14-helix-bundle formation by beta-peptides. Org. Lett. **10**(9), 1799–1802 (2008)
58. D.S. Daniels et al., High-resolution structure of a beta-peptide bundle. J. Am. Chem. Soc. **129**(6), 1532–1533 (2007)
59. E.J. Petersson et al., Biophysical characterization of a beta-peptide bundle: comparison to natural proteins. J. Am. Chem. Soc. **129**(17), 5344–5345 (2007)
60. W.C. Pomerantz et al., Lyotropic liquid crystals formed from ACHC-rich beta-peptides. J. Am. Chem. Soc. **133**(34), 13604–13613 (2011)
61. T.L. Raguse et al., Structure-activity studies of 14-helical antimicrobial beta-peptides: probing the relationship between conformational stability and antimicrobial potency. J. Am. Chem. Soc. **124**(43), 12774–12785 (2002)
62. A.J. Karlsson et al., Antifungal activity from 14-helical beta-peptides. J. Am. Chem. Soc. **128**(39), 12630–12631 (2006)
63. R. Akkarawongsa et al., Inhibition of herpes simplex virus type 1 infection by cationic beta-peptides. Antimicrob. Agents Chemother. **52**(6), 2120–2129 (2008)
64. B.P. Mowery et al., Mimicry of antimicrobial host-defense peptides by random copolymers. J. Am. Chem. Soc. **129**(50), 15474–15476 (2007)
65. M.W. Lee et al., Two interdependent mechanisms of antimicrobial activity allow for efficient killing in nylon-3-based polymeric mimics of innate immunity peptides. Biochim. Biophys. Acta **1838**(9), 2269–2279 (2014)

66. B.P. Mowery et al., Structure-activity relationships among random nylon-3 copolymers that mimic antibacterial host-defense peptides. J. Am. Chem. Soc. **131**(28), 9735–9745 (2009)
67. S. Chakraborty et al., Effects of cyclic vs. acyclic hydrophobic subunits on the chemical structure and biological properties of Nylon-3 co-polymers. ACS Macro Lett. **2**(8), 753–756 (2013)
68. R. Liu et al., Nylon-3 polymers with selective antifungal activity. J. Am. Chem. Soc. **135**(14), 5270–5273 (2013)
69. L.A. Rank et al., A cationic polymer that shows high antifungal activity against diverse human pathogens. Antimicrob. Agents Chemother. **61**(10), e00204–e00217 (2017)
70. L.A. Rank et al., Peptide-like Nylon-3 polymers with activity against phylogenetically diverse, intrinsically drug-resistant pathogenic fungi. mSphere **3**(3), 3845–3852 (2018)